Earth Planet. Sci. Lett. 622 (2023) 118422

Contents lists available at ScienceDirect

Earth and Planetary Science Letters

journal homepage: www.elsevier.com/locate/epsl

New paleomagnetic data from the central Tethyan Himalaya refine the size of Greater India during the Campanian

Jie Yuan [a], Chenglong Deng [a,b,*], Zhenyu Yang [c], Wout Krijgsman [d], Thubtantsering [e], Huafeng Qin [a,b], Liang Yi [f], Pan Zhao [a], Bo Wan [a,b], Liang Zhao [a,b], Huaiyu He [a,b], Zhengtang Guo [g], Rixiang Zhu [a,b]

[a] State Key Laboratory of Lithospheric Evolution, Institute of Geology and Geophysics, Chinese Academy of Sciences, Beijing 100029, China
[b] College of Earth and Planetary Sciences, University of Chinese Academy of Sciences, Beijing 100049, China
[c] College of Resources, Environment and Tourism, Capital Normal University, Beijing 100048, China
[d] Department of Earth Sciences, Utrecht University, Utrecht, HD 3584, The Netherlands
[e] College of Science, Tibet University, Lhasa 850000, China
[f] State Key Laboratory of Marine Geology, Tongji University, Shanghai 200092, China
[g] Key Laboratory of Cenozoic Geology and Environment, Institute of Geology and Geophysics, Chinese Academy of Sciences, Beijing 100029, China

ARTICLE INFO

Keywords:
Greater India
Tethyan Himalaya
Upper Cretaceous oceanic red beds
High-resolution thermal demagnetization
India-Asia collision system

ABSTRACT

Knowledge of the size of Greater India is critical to deciphering the geodynamic processes of the India-Asia collision, as the size of this landmass primarily determines the amount of continental subduction and crustal shortening. Recently, paleomagnetic data revealed the rapid drift of a Himalayan microcontinent (i.e., the Tibetan Himalaya) during ca. 75–61 Ma, which resulted in a triple-stage India-Asia collision scenario. This scenario implies a relatively small Greater India at 75 Ma (Late Cretaceous), but this hypothesis is only based on one high quality Campanian paleomagnetic pole from the eastern part of the Tethyan Himalaya. Here we report comprehensive petrographic, rock magnetic and paleomagnetic studies on Upper Cretaceous oceanic affinity red beds (CORBs) of the Chuangde Formation from the central part of the Tethyan Himalaya at 83.6°E longitude. These CORBs are characterized by multi-component magnetizations carried dominantly by detrital hematite, which retains a primary remanent magnetization. Accordingly, the high temperature magnetization components (585–690°C) were isolated by high-resolution thermal demagnetization. The new paleomagnetic data provide, after applying an inclination shallowing correction, a Campanian paleopole of 43.3°N/258.3°E, which places the central part of the Tethyan Himalaya at a paleolatitude of 16.7° ± 1.8°S at ca. 75 Ma. Comparison of this paleolatitude with the expected paleolatitude of India, using its apparent polar wander path, shows that the N-S extent of central Greater India was ~910 km during the middle Campanian. Our paleomagnetic data are in agreement with balanced cross section reconstructions and seismologic interpretations of the India-Asia collision zone and provide additional support for the North India Sea hypothesis. The improved estimate of the size of Greater India has several implications for Indian continental crust behavior and results in an updated reconstruction of the India-Asia collision system in the Campanian.

1. Introduction

Greater India (Argand, 1924) is a nearly 100-yr-old concept that has been used in tectonic models of the India-Asia collision system (Powell et al., 1988; Ali and Aitchison, 2005; Copley et al., 2010; Ding et al., 2017, 2022; Hu et al., 2017; Meng et al., 2019; Dannemann et al., 2022; van Hinsbergen, 2022). It refers to the ancient northern margin of India that originally extended farther north and has been subducted and tectonically shortened during the India-Asia collision and subsequent intra-continental convergence. Accurately quantifying the size of Greater India is a key boundary condition for reconstructing the Tethyan paleogeography (Ali and Aitchison, 2005; van Hinsbergen et al., 2019; Zhu et al., 2022), delineating the geodynamic process of the India-Asia collision (Yin, 2006; Aitchison et al., 2007; van Hinsbergen et al., 2012;

* Corresponding author at: State Key Laboratory of Lithospheric Evolution, Institute of Geology and Geophysics, Chinese Academy of Sciences, Beijing 100029, China.
E-mail address: cldeng@mail.iggcas.ac.cn (C. Deng).

https://doi.org/10.1016/j.epsl.2023.118422
Received 29 January 2023; Received in revised form 14 August 2023; Accepted 24 September 2023
Available online 6 October 2023

Ding et al., 2017; Kapp and DeCelles, 2019; Yuan et al., 2021, 2022; Dannemann et al., 2022), and clarifying how Indian continental lithosphere behaved in the India-Asia collision system (Powell et al., 1988; Xiao et al., 2017; van Hinsbergen, 2022). These issues are all of great significance for understanding the rise and growth of the Himalayas and the Tibetan Plateau (Molnar and Tapponnier, 1975; Yin, 2006; Ding et al., 2022).

The estimates of Greater India can be mainly divided into two groups, resulting in two kinds of India-Asia collision scenarios: the single-stage collision model and the two-stage collision model. The traditional single-stage collision model (Yin and Harrison, 2000; Ingalls et al., 2016; Meng et al., 2019) requires a Greater India with an extent of >2000 km and is consistent with the observation of only one suture zone in the Himalayas. This model also explains the arrival of Asian sediments in the Tethyan Himalaya at ca. 60 Ma. The single-stage model is, however, not consistent with plate circuit reconstructions and the magnitude of documented shortening.

In contrast, the two-stage collision models all invoke a much smaller extent of Greater India (roughly < 1000 km) and infer two suture zones in the Himalayas: 1) the island arc-continent collision model (Aitchison et al., 2007; Jagoutz et al., 2015; Westerweel et al., 2019; Martin et al., 2020) proposes the collision of Greater India with an intra-oceanic arc that developed within the Neo-Tethys Ocean at ca. 50 Ma before an ocean basin was consumed to the north until ca. 40 Ma. This model satisfies plate circuit reconstructions, magnitude of documented shortening and rapid India-Asia convergence, but fails to explain the arrival of Asian detritus in the Tethyan Himalaya at ca. 60 Ma; 2) the India-arc collision with the Xigaze backarc basin model (Kapp and DeCelles, 2019), invokes rifting of (part of) the Gangdese arc and its forearc to open a backarc basin at ca. 90–70 Ma. This rifted arc collided first with Greater India at ca. 60 Ma before the backarc basin closed at ca. 45 Ma. It explains the arrival of Asian sediments in the Tethyan Himalaya at ca. 60 Ma, concurs with plate circuit reconstructions and magnitude of documented shortening, but lacks direct geologic evidence for the opening and closure of the Xigaze backarc basin; 3) the Greater India Basin model (van Hinsbergen et al., 2012, 2019) specifically invokes rifting of the Tibetan Himalaya (that is, the Tethyan Himalaya plus the Greater Himalaya) from India to open an intervening ocean basin between ca. 120 Ma and ca. 25 Ma. This model fulfils plate circuit reconstructions and magnitude of documented shortening, but fails to explain why Asian and Tethyan Himalaya detritus reaches the Lesser Himalaya and sub-Himalaya at ca. 55−45 Ma; 4) the North India Sea model (Yuan et al., 2021) invokes rifting of the Tibetan Himalaya away from India, but generating an ocean basin during ca. 75−53/48 Ma. It predicts the arrival of Asian sediments in Tethyan Himalaya formations at ca. 60 Ma and the arrival of Asian and Tethyan Himalaya sediments in Lesser Himalaya and sub-Himalaya formations at ca. 55−45 Ma. This model concurs with plate circuit reconstructions and magnitude of documented shortening, but still lacks unambiguous geologic evidence to support the presence of such an ocean basin.

Recently, a triple stage collision was proposed (Yuan et al., 2022), which involved an arc-continent collision (Martin et al., 2020) followed by a two-stage continent-continent collision (Yuan et al., 2021). Paleomagnetic data that underlie the triple stage collision model place the Tethyan Himalaya microcontinent at paleolatitudes of ~19.4°S at ca. 75 Ma and ~14.1°N at ca. 61 Ma, respectively (Yuan et al., 2021, 2022). These data imply that the Tibetan Himalaya) drifted northward with an anomalously high speed of ~263 mm/year during the interval ca. 75−61 Ma while India itself moved at a much slower speed of ~100 mm/year, as determined from its apparent polar wander path during the interval 80−60 Ma (Torsvik et al., 2012). The large speed difference led Yuan et al. (2021, 2022) to hypothesize that the Tibetan Himalaya rifted away from India after ca. 75 Ma, generating the North India Sea.

In the triple stage collision scenario, the paleogeographic reconstruction of Greater India during the Late Cretaceous (ca. 75 Ma: Campanian) is only based on one high quality paleomagnetic pole, that of Yuan et al. (2021), from the eastern part of the Tethyan Himalaya. However, paleomagnetic data from the eastern Tethyan Himalaya cannot effectively define the entire Greater India extent, allowing alternative hypotheses that its central part may have had a >2400 km promontory (Meng et al., 2019). It is thus important to obtain reliable Late Cretaceous paleomagnetic data from the central and western parts of the Tethyan Himalaya. To this end, we conducted paleomagnetic and rock magnetic investigations, and scanning electron microscopy (SEM) observations on the Upper Cretaceous oceanic red beds (CORBs) of the Chuangde Formation exposed at the Pianji section (29°45.22′N, 83°35.79′E). These strata are interpreted to have been deposited on the distal part of the Indian passive margin, corresponding to the central part of the Tethyan Himalaya (Du et al., 2015). Our new paleomagnetic results provide a key estimate of the ca. 75-Ma Greater India extent at its central part. We also analyze multiple lines of geologic and geophysical evidence for the refined size of Greater India and its implication for the Tethyan paleogeography, the India-Asia collision, and the behavior of Indian continental crust.

2. Geologic setting and sampling

2.1. Geologic setting

The Himalaya orogen comprises four tectonostratigraphic units, from north to south including the Tethyan Himalaya, the Greater Himalaya, the Lesser Himalaya and the Sub-Himalaya, which are separated by the South Tibet Detachment System, the Main Central Thrust and the Main Boundary Thrust, respectively (Yin, 2006) (Fig. 1a). The Tethyan Himalaya was formed in a passive continental margin setting and can be divided into the northern and southern subzones of different lithologic compositions by the Gyirong-Kangmar thrust (Liu and Einsele, 1994). The southern subzone is characterized by Paleozoic to Eocene shallow-water calcareous and terrigenous sedimentary rocks of continental shelf settings (Liu and Einsele, 1994), while the northern subzone is mainly composed of Mesozoic to Paleogene deep-water siliciclastic and terrigenous sedimentary rocks of outer shelf and continental slope settings (Liu and Einsele, 1994; Chen et al., 2011; Li et al., 2011).

The Jurassic−Upper Cretaceous strata of the northern subzone, exposed at the Pianji section in Zhongba, consist of four formations: the Upper Jurassic Weimei Formation, the Lower Cretaceous Rilang Formation, the Lower−Upper Cretaceous Duobeng Formation and the Upper Cretaceous Chuangde Formation (Du et al., 2015) (Figs. 1a, b and c). Du et al. (2015) described the stratigraphy and petrography of the Pianji section from oldest to youngest: 1) the Weimei Formation is ~25 m thick and mainly composed of quartz sandstones; 2) the Rilang Formation is also ~25 m thick and consists of medium to fine-grained volcaniclastic rocks; 3) the Duobeng Formation is ~35 m thick and comprises radiolarian cherts and siliceous shales, and was dated to be the Barremian to Aptian age (ca. 131−110 Ma) by radiolarians (Li et al., 2017); 4) the Chuangde Formation is ~31 m thick and comprises violet-red shales intercalated with thin marlstone beds. A parallel (tectonic) unconformity is present between the Duobeng Formation and the Chuangde Formation.

The Chuangde Formation CORBs can be stratigraphically correlated across southern Tibet (Chen et al., 2011; Du et al., 2015). They are considered deep-water terrigenous sediments that were accumulated under relatively oxidic conditions following an environmental recovery after anoxia in the world's oceans (Chen et al., 2011; Li et al., 2011). Detailed investigations of its planktonic foraminifers in Gyangze indicate an early to middle Campanian age (Chen et al., 2011). Radiolarians retrieved from the Chuangde Formation in Kangmar also indicate a Campanian age (Li et al., 2011). Recently, the Cailangba CORBs in Gyangze were magnetobiostratigraphically defined to the time interval of ca. 76.2−74.0 Ma (Yuan et al., 2021). Thus, based on these regional biostratigraphic and magnetostratigraphic correlations, we infer that

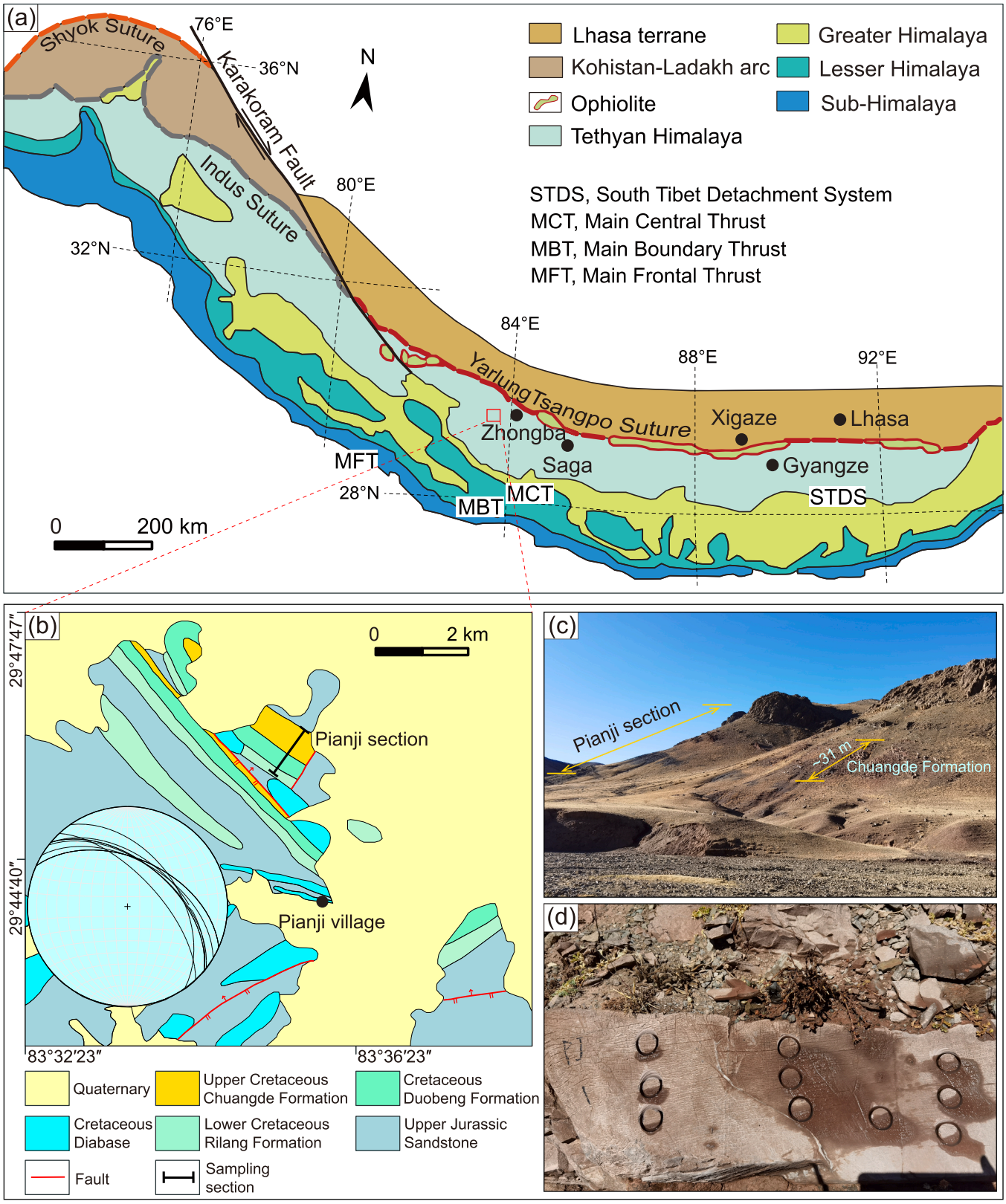

Fig. 1. Geologic map of the study region. (a) Geologic map of the Himalaya, simplified from Yin (2006). (b) Geologic map of the studied Pianji section and adjacent regions, simplified from Meng et al. (2019). (c) A field photo showing the strata exposed at the Pianji section. (d) The Upper Cretaceous oceanic red beds (CORBs) of the Chuangde Formation with positions of drill cores.

the Chuangde Formation CORBs in Zhongba was also deposited in the middle Campanian, so roughly between ca. 76 and ca. 74 Ma.

2.2. Sampling

We drilled 106 core samples at 11 sites from red shales and marlstones of the Chuangde Formation at the Pianji section in Zhongba using a gasoline-powered portable drill. The bedding orientation at the sampled section is roughly uniform in strike and dip (Fig. 1b). Sites PJ1−PJ11 have a strike range from 294° to 325° and a dip range from 47° to 65°. In order to test for the potential influence of depositional and/or compaction-induced inclination shallowing, three hand samples oriented on the stratigraphic bedding were collected from different levels. All the core samples were oriented with both magnetic and sun compasses. The samples were cut into 147 standard specimens with a length of 2.2 cm in the laboratory for thermal demagnetization experiments. The remaining parts were used for rock magnetic analyses and SEM observations.

3. Methods

3.1. Magnetic mineralogy

3.1.1. SEM observations

Polished thin sections were investigated using the SEM to determine the microscopic shape and microstructure of magnetic minerals. Backscattered electron microscopy analyses were carried out using a SEM (FEI Nova NanoSEM 450) with an energy dispersive spectrometer (EDS) (Oxford X-MAX80).

3.1.2. Rock magnetism

To identify the magnetic remanence carriers, 10 representative samples were selected for rock magnetic measurements, including hysteresis loops, isothermal remanent magnetization (IRM) acquisition curves and backfield demagnetization curves. Also, hysteresis loops were applied in cycled fields with a maximum of 1.5 T. Saturation magnetization (M_s), saturation remanence (M_{rs}), and coercivity (B_c) were calculated after high-field slope correction. The IRM acquisition curves were obtained in fields from 0 to 1.5 T. The coercivity of remanence (B_{cr}) was obtained by stepwise demagnetization of the saturated isothermal remanent magnetization (SIRM) in a backfield up to −1.5 T. Magnetic components were analyzed using the method of unmixing developed by Kruiver et al. (2001).

Six representative specimens were magnetized in progressively smaller fields (2.5, 0.5, and 0.15 T) along three perpendicular directions (Z-axis, Y-axis, and X-axis), respectively, using a 2G Enterprises Pulse Magnetizer (2G660) (Lowrie, 1990). These specimens were then processed to progressive thermal demagnetization up to 680°C with 10−100°C intervals, using a PGL-100 thermal demagnetizer of Qin et al. (2020).

Anisotropy of magnetic susceptibility (AMS) measurements were made using a KLY-4s Kappabridge before thermal demagnetization.

3.2. Demagnetization of the natural remanent magnetization (NRM)

All 147 specimens of the Pianji section were subjected to high-resolution thermal demagnetization up to 670−690°C with 20−50°C intervals from room temperature to 585°C, with 10°C intervals from 585°C to 650°C and with 5°C intervals from 650°C to 690°C using a PGL-100 thermal demagnetizer (Qin et al., 2020). The remanences were measured on a 2-G Enterprises Model 755 cryogenic magnetometer installed inside a magnetically shielded space with background field of less than 300 nT. The principal component analysis was computed by least-squares fits (Kirschvink, 1980). The mean directions were analyzed using classic Fisher statistics (Fisher, 1953).

4. Results

4.1. Magnetic mineralogy

4.1.1. SEM observations

The SEM observations of two selected samples are shown in Fig. 2. They reveal two types of hematite grains with different shapes and origins. One type features a relatively large particle size (~5−20 μm) with triangular, rectangular, rhombic and irregular shapes (Fig. 2a−i and k−l). This type of hematite is interpreted to be of detrital origin. The other type has a smaller particle size (<1 μm) and shows acicular and subhedral to euhedral morphologies. This type of hematite is grown in pores (Fig. 2d, j) or along fractures (Fig. 2a, e, g and k) and is interpreted to be of chemical (authigenic) origin. The SEM observations thus indicate that the magnetic mineral assemblage consists of both detrital and chemical hematite grains.

4.1.2. Thermal demagnetization of three-component IRM

Stepwise thermal demagnetization of the three orthogonal component IRM (Lowrie, 1990) is effective in revealing the laboratory unblocking temperature range of the magnetic remanence carriers. Thermal demagnetization of three-component IRM shows that the hard and intermediate magnetization components decreased rapidly over a temperature range of 650−680°C and finally unblocked at 685°C (Fig. 3). This suggests that high-coercivity hematite dominates the magnetic remanence carrier in the CORBs of the Pianji section.

4.1.3. Hysteresis properties, IRM acquisition curves and backfield demagnetization curves

Hysteresis curves generally show rectangular loops (Fig. 4a−c) that are closed above 1.5 T, characteristic of hematite. The IRM acquisition curves indicate that the magnetic remanence is still not saturated at the maximum applied field of 1.5 T. The B_{cr} values (defined with respect to 1.5 T) are as large as 441−478 mT. Component analyses of coercivity distributions (Kruiver et al., 2001) show two components with different coercivities, indicative of two different assemblages of hematite grains (Fig. 4d−f). Component 1 with median acquisition field ($B_{L1/2}$) of 158.5 mT contributes 5%−13% to the SIRM, and is interpreted to reside in fine-grained chemical hematite (Fig. 4d−f). Component 2 with median acquisition field ($B_{H1/2}$) of 589−617 mT contributes 87%−95% to the SIRM, and is interpreted to be carried by coarse-grained detrital hematite (Fig. 4d−f). All these rock magnetic experiments indicate that the dominant magnetic mineral is high-coercivity hematite of coarse-grained nature and detrital origin.

4.1.4. AMS

AMS data are shown in equal area projections and indicate a consistent clustering of results (Fig. 5). In stratigraphic coordinates, the maximum k1 and intermediate k2 principle anisotropy directions lie in the bedding plane with well grouped magnetic lineations; minimum k3 directions are essentially perpendicular to the bedding (Fig. 5b). Magnetic susceptibility (K_m) values range from 1.57×10^{-5} SI to 7.36×10^{-5} SI (Fig. 5c). P_j values vary from 1.051 to 1.142, with an average of 1.094 (Fig. 5c). The AMS data show a magnetic fabric that is dominated by oblate ellipsoids (Fig. 5d), suggesting that the sedimentary magnetic fabrics have not been subjected to any form of progressive, penetrative deformation (e.g., Yuan et al., 2021).

4.2. Paleomagnetic results

Thermal demagnetization diagrams show complex behavior and the presence of at least three different magnetization components, a low laboratory unblocking temperature component (LTC), a middle-temperature component (MTC) and a high-temperature component (HTC) (Fig. 6). The LTCs from 147 specimens were isolated in the temperature interval between 20°C and 250°C (Fig. 6). The overall mean

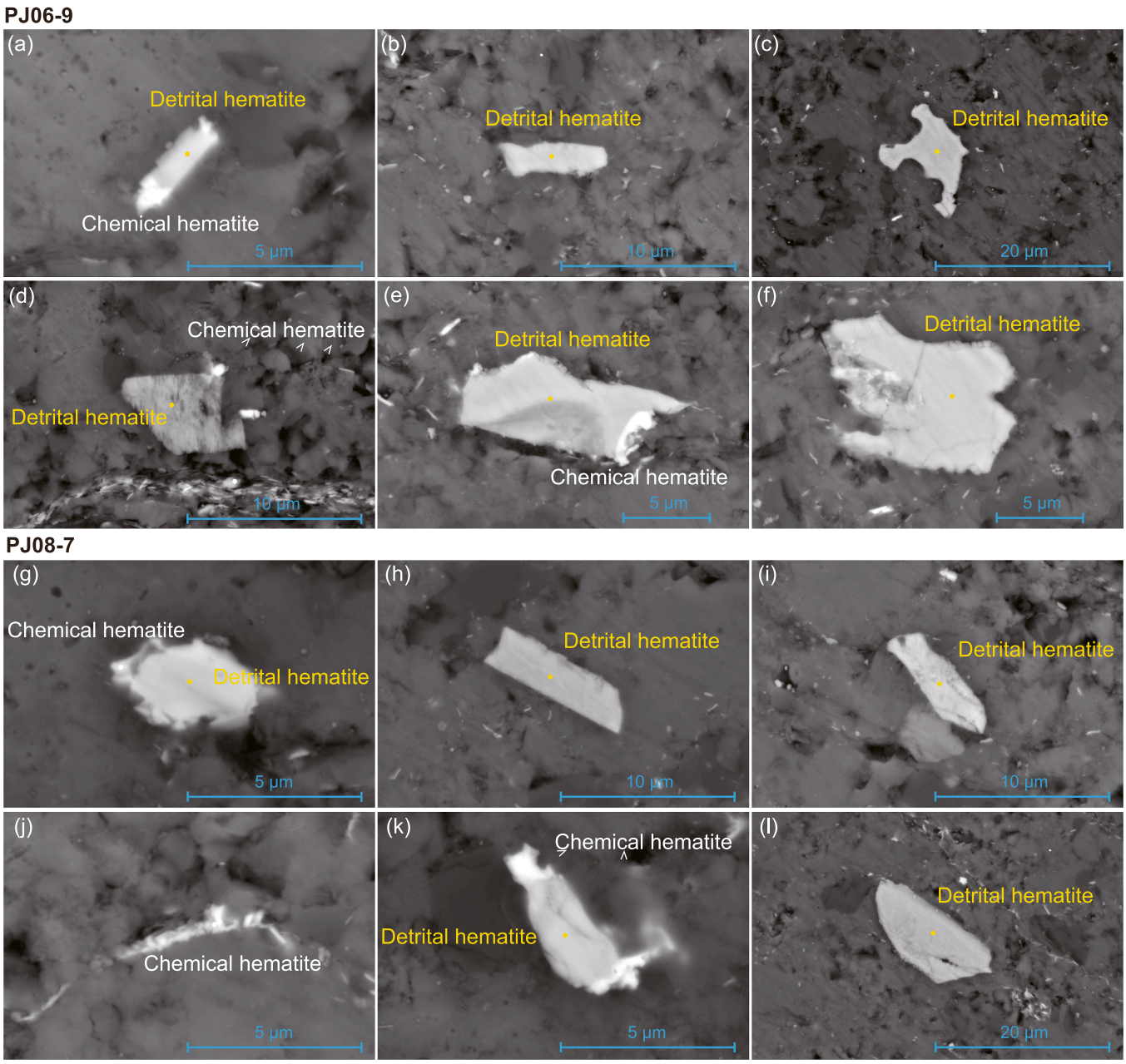

Fig. 2. Scanning electron microscope (SEM) backscattered electron images. The yellow and white dots indicate energy dispersive spectrometer analysis spots.

direction of the LTCs is $D_g = 356.2°$, $I_g = +46.2°$, $k = 150.2$, $\alpha_{95} = 1.0°$, $n = 147$ (specimens) before tilt correction, and $D_s = 10.3°$, $I_s = +1.6°$, $k = 81.6$, $\alpha_{95} = 1.3°$ after tilt correction (Fig. 7a, b). The sample-mean direction before tilt correction is close to the present geomagnetic field direction ($D = 0.7°$, $I = +47.0°$) and the geocentric axial dipole direction ($D = 0°$, $I = +48.9°$) of the sampling area, indicating that the LTCs are viscous remanent magnetizations.

The MTCs were isolated in the temperature interval of 450–585°C from 147 specimens (Fig. 6). The corresponding sample-mean direction is $D_g = 12.9°$, $I_g = -19.2°$, $k = 42.5$, $\alpha_{95} = 1.8°$, $n = 147$ (specimens) before tilt correction, and $D_s = 342.1°$, $I_s = -60.9°$, $k = 29.1$, $\alpha_{95} = 2.2°$ after tilt correction (Fig. 7c, d). The precision parameter (k) decreases from 42.5 to 29.1 after tilt correction, suggesting that the MTCs are probably post-folding magnetizations. We tentatively speculate that the MTC magnetization was acquired during a normal polarity chron soon after deposition.

The HTCs were isolated from 116 specimens (10 sites) (Table S1). All the HTCs were isolated in the temperature interval between 585°C and 690°C, with laboratory unblocking temperatures between about 660°C and 690°C (Fig. 6). The sample-mean direction of the HTCs is $D_g = 184.6°$, $I_g = -21.2°$, $k = 43.0$, $\alpha_{95} = 2.0°$, $n = 116$ (specimens) before tilt correction, and $D_s = 184.0°$, $I_s = +22.8°$, $k = 51.7$, $\alpha_{95} = 1.8°$ after tilt correction (Fig. 7e, f).

Rock magnetic behaviors and SEM observations document that the MTCs and the HTCs are mainly carried by fine-grained authigenic hematite and coarse-grained detrital hematite, respectively. Following the Néel relaxation theory, there is a strong relationship between grain volume and unblocking temperature, which can be used to estimate grain size (Néel, 1949; Swanson-Hysell et al., 2019). Applying this relation, we infer the MTCs that were unblocked from 450°C up to 585°C (Fig. 6) are likely carried by authigenic pigmentary hematite grains within the ~150–220 nm size range; the HTCs with unblocking temperatures up to 690°C (Fig. 6) are dominantly held by detrital hematite grains larger than 220 nm. We conclude that the MTCs represent

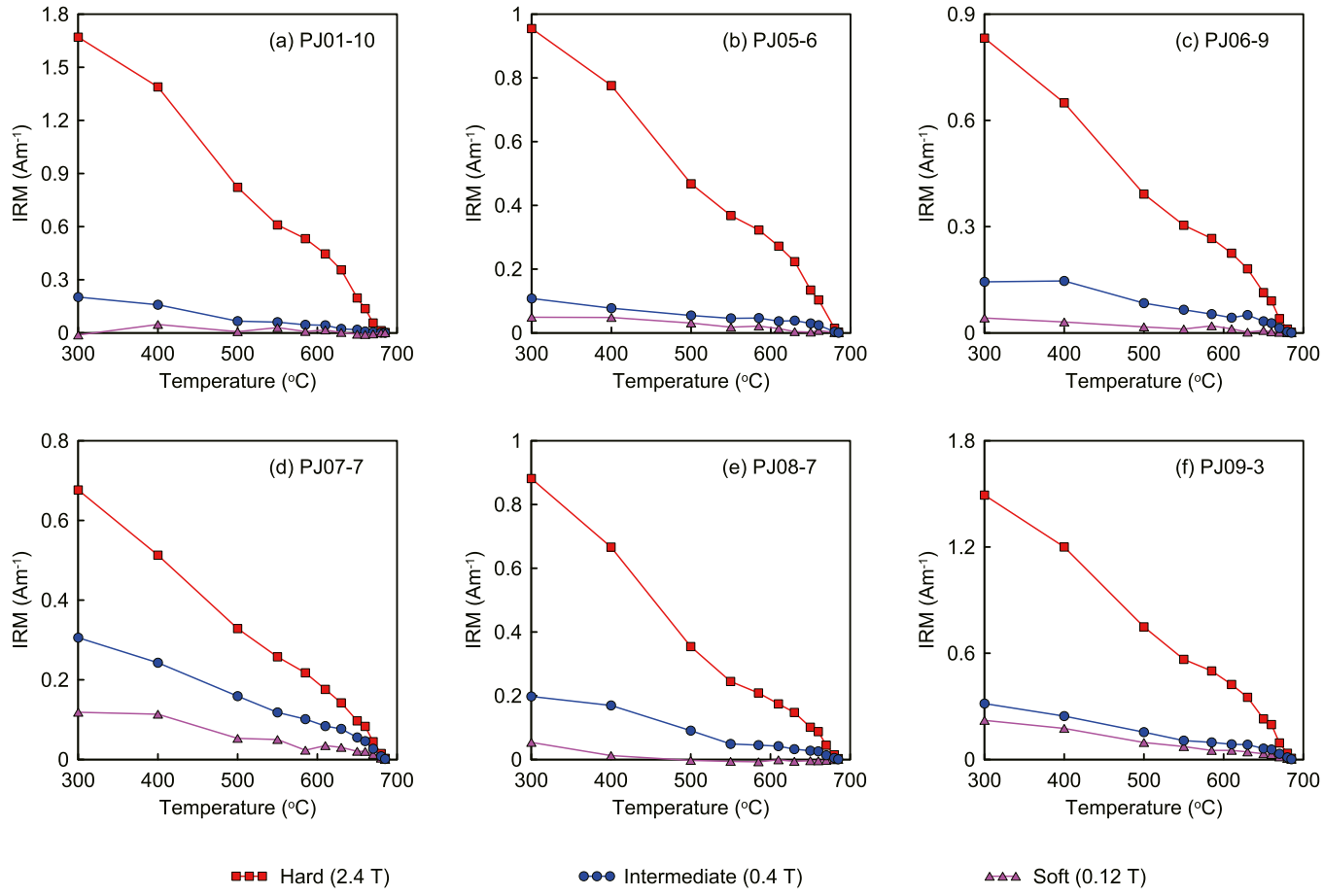

Fig. 3. Thermal demagnetization of the three-component IRM imparted with direct current fields of 2.4 T, 0.4 T, and 0.12 T along three perpendicular axes. The curves below 300°C were omitted for reasons of clarity.

remagnetization components, that are of chemical origin, probably formed via the influence of orogenic hydrothermal fluids (Swanson-Hysell et al., 2019); and that the HTCs are most likely primary magnetizations, again carried by detrital hematite.

4.3. Reliability of the paleomagnetic data

We document a primary origin for the HTCs of the Chuangde Formation CORBs from the Pianji section based on the following lines of evidence. First, the rock magnetic results and SEM observations indicate that the coarse-grained hematite is of primary detrital origin. Second, the MTCs are unblocked around 585°C, but the HTCs are unblocked around 680°C (Fig. 6), and we thus have successfully isolated the contribution of secondary chemical remanent magnetization. Third, the fold tests (Watson and Enkin, 1993; Enkin, 2003) on the HTCs are positive when performed at the specimen level (Fig. 8a, c). Additionally, the confidence ranges from 74% to 108% for the parametric bootstrap fold test of Tauxe and Watson (1994). Fourth and finally, Yuan et al. (2021) reported paleomagnetic results of the Chuangde Formation CORBs from the Cailangba section near Gyangze, ~800 km to the east of the present study area (Fig. 1). Notably, the bedding attitudes at these two localities are slightly different, permitting a regional fold test. Combining our new data with those of Yuan et al. (2021), the regional fold tests (Watson and Enkin, 1993; Enkin, 2003) are also positive when performed at the specimen level (Fig. 8b, d). The confidence interval is between 70% and 91% for the parametric bootstrap fold test of Tauxe and Watson (1994). Furthermore, the sample-mean direction of the HTCs from the Pianji section in this study and the Cailangba section of Yuan et al. (2021) passes the regional fold tests of McElhinny (1964) and McFadden (1990) at 95% confidence level. The increase of precision parameter k after tilt correction ($k_s/k_g = 1.18 > F(484, 484) = 1.16$) is consistent with a positive fold test of McElhinny (1964) at the 95% confidence level. In the fold test of McFadden (1990), the calculated values are $\xi_{(2)\text{in situ}} = 85.79$ in geographic coordinates and $\xi_{(2)\text{tilt corrected}} = 10.00$ after tilt correction, while the critical value is $\xi_C = 18.13$ at 95% confidence level, also indicating a positive fold test.

4.4. Inclination shallowing correction

Depositional and post-depositional compaction processes may have induced inclination shallowing in red beds and other sedimentary rocks (Tauxe and Kent, 2004). The IRM anisotropy-based inclination correction (Hodych and Buchan, 1994) and the elongation/inclination (E/I) correction (Tauxe and Kent, 2004) are two frequently used methods in paleomagnetism to correct for potential inclination shallowing. We use these two methods to test the inclination shallowing of the remanence of the studied CORBs.

Three hand samples from three different stratigraphic levels, oriented on the bedding plane, were used for anisotropy-based inclination correction. A total of 12 specimens were drilled from these hand samples in the direction perpendicular to the stratigraphic bedding and then subjected to experiments using methods as described in Yuan et al. (2021) (Fig. 9). As a result, the values of IRMz/IRMx (IRM perpendicular/IRM parallel) of 12 specimens in the range of 200−1000 mT changed from 0.6720 to 0.7481, while those of IRMz/IRMx in the thermal demagnetization temperature interval of 585−685°C changed from 0.6249 to 0.7373, respectively (Fig. 9; Table S2). Considering the HTCs are unblocked over the temperature interval of 585°C to 685°C,

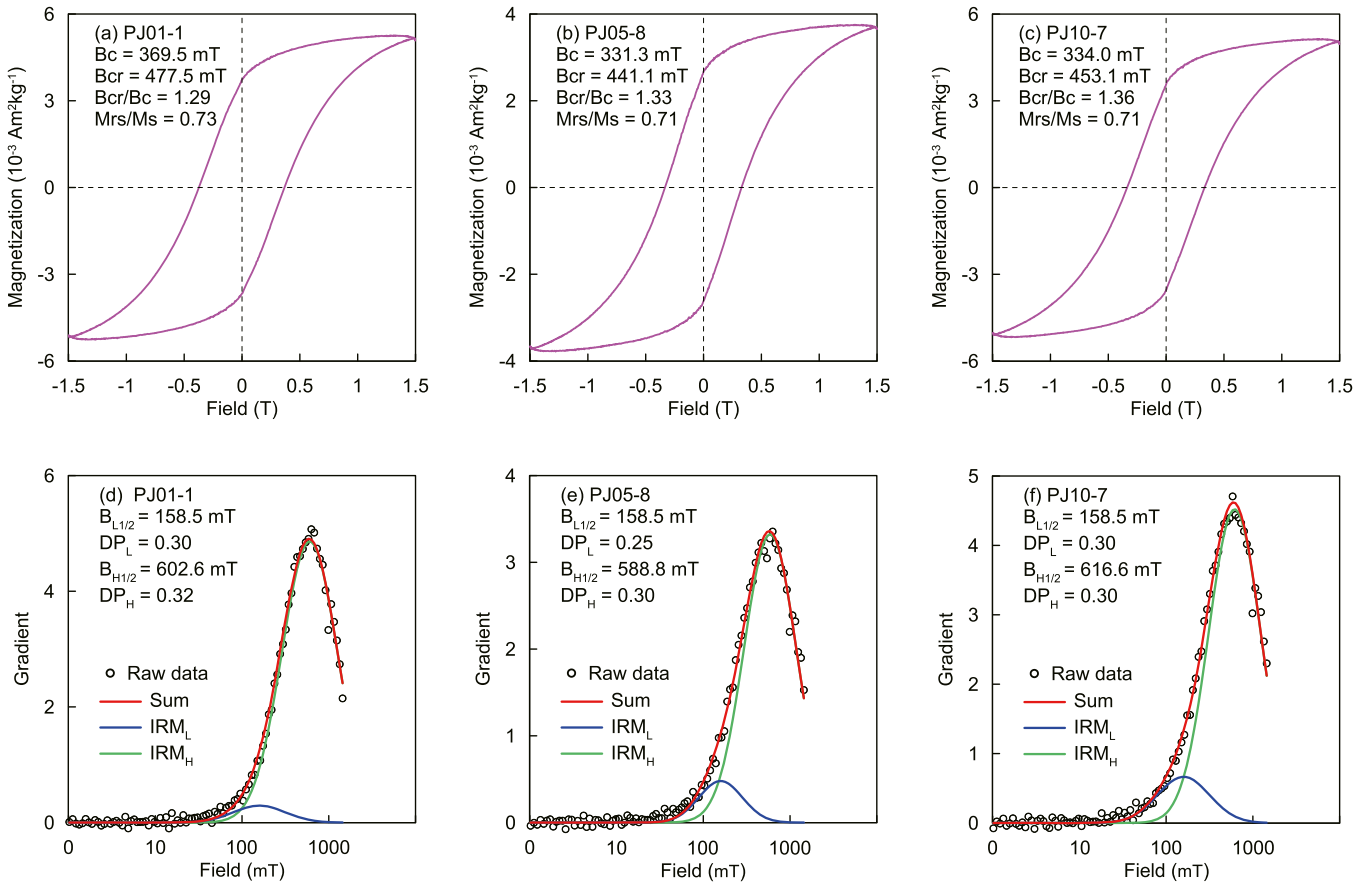

Fig. 4. Rock magnetic properties. (a–c) Hysteresis loops after high-field slope correction with hysteresis parameters indicated. (d–f) Component analysis of coercivity distributions with blue, green and red lines indicating the low coercivity component (IRM_L), high coercivity component (IRM_H) and the sum of these components (Sum), respectively. $B_{1/2}$ is the field at which half of the saturation IRM (SIRM) is reached; and the dispersion parameter (DP) represents one standard deviation (Robertson and France, 1994). $B_{L1/2}$ and $B_{H1/2}$ represent $B_{1/2}$ of the low- and high-coercivity components, respectively. DP_L and DP_H represent DP of the low- and high-coercivity components, respectively. Open circles indicate raw IRM gradient data (raw data).

the mean IRMz/IRMx of each specimen in the temperature range of 585 to 685°C was used to calculate the mean IRMz/IRMx of the sampling section and this is ~0.7. The sample-mean inclination of the studied CORBs of the Pianji section increased from +22.8° to +31.0° after the IRM anisotropy-based inclination correction.

The strongly elongated distribution of the HTCs (Fig. 9h) is also an indication that inclination flattening may have played a significant role. The sample-mean direction of all the HTCs from the Pianji section is D_s = 184.0°, I_s = +22.8°, k = 51.7, α_{95} = 1.8°, n = 116 after tilt correction (Fig. 9h). After application of the E/I correction on all the HTCs from the Pianji section (n = 116 specimens), the corresponding E/I corrected inclination increases from 22.8° to 46.4°, with the best estimate between 37.0° and 59.2° at the 95% confidence level (Fig. 9i). However, a relatively small number of specimens from sites PJ5–PJ8 (Fig. 9j) that have a nearly uniform bedding orientation, yield a mean direction of D_s = 188.9°, I_s = +22.3°, k = 78.4, α_{95} = 2.2°, n = 54 after tilt correction (Fig. 9k). After application of the E/I correction on the HTCs of sites PJ5–PJ8 (n = 54 specimens), the corresponding E/I corrected inclination increases from 22.3° to 38.7°, with the best estimate between 29.4° and 53.6° at the 95% confidence level (Fig. 9l). The IRM anisotropy-based corrected inclination is +31.0°, which also falls within the best estimate.

In addition, Yuan et al. (2021) used the IRM anisotropy-based inclination correction (Hodych and Buchan, 1994) and the E/I correction (Tauxe and Kent, 2004) to test for inclination shallowing of the CORBs of the Cailangba section at Gyangze, which both yield a shallowing factor of ~0.7. Due to the tectonostratigraphic and lithologic equivalence of the Chuangde Formation CORBs at both Gyangze and Zhongba, the measured sample-mean inclination of the studied CORBs from the Pianji section was corrected with the IRM anisotropy-based shallowing factor of ~0.7, which gives a paleopole of 43.3°N/258.3°E, A_{95} = 1.8°, with a paleolatitude of 16.7° ± 1.8°S. We conclude that the primary magnetization of ca. 75 Ma vintage was acquired during a reverse polarity chron.

5. Discussion

5.1. The extent of Greater India during the middle Campanian

Ali and Aitchison (2005) provided a comprehensive review of previous Greater India models and concluded that the longest N-S extension of Greater India is about 8.5° along a great circle, including the area of Himalayas. Recently, Ding et al. (2017) suggested that Greater India only includes the tectonically shortened and subducted portions of the Indian continental crust, excluding the area of Himalayas with a latitudinal width of ~2.5°. In this study, we adopt the definition of Greater India proposed by Ding et al. (2017), who state that "*GI (Greater India) can thus be defined as the region to the north of the Indian plate, including under thrusted Indian lithosphere and crustal shortening in the Himalayan mountain belt*".

The anticlockwise rotation of the Indian continent during the Early Cretaceous implies that the magnitude of the Greater India extent in the present N-S direction is larger than the derived difference of the observed and expected paleolatitudes (Bian et al., 2022). However, the

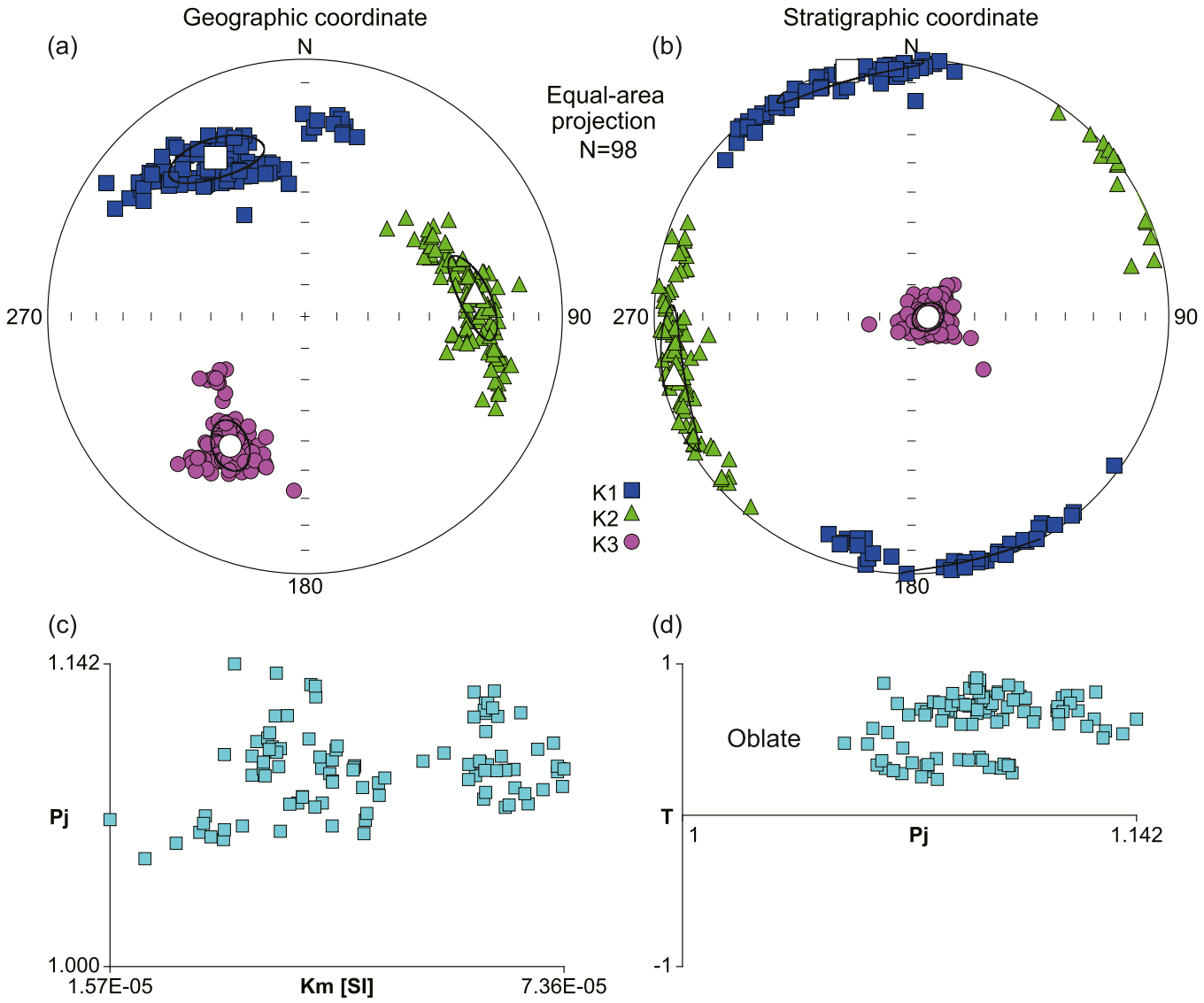

Fig. 5. Magnetic fabric data. (a, b) Equal-area projections of the maximum (blue squares), intermediate (green triangles) and minimum (purple circles) susceptibility axes in geographic (a) and stratigraphic (b) coordinates. (c) Magnetic susceptibility (K_m) versus anisotropy (P_j) plot. (b) Anisotropy (P_j) versus shape parameter (T) plot. Solid symbols, individual specimen directions; larger open symbols, mean directions with 95% confidence limit.

Indian continent rotated to a nearly N-S (present-day) orientation after ca. 80 Ma. Thus, at ca. 75 Ma the effect of anticlockwise rotation of India on determining the size of Greater India is negligible, in fact, almost nonexistent. Our new paleomagnetic results from ca. 75 Ma rocks from the central part of the Tethyan Himalaya yield a paleolatitude of 16.7° ± 1.8°S for the most distal Indian continental margin (Fig. 10), while an expected paleolatitude of 25.0° ± 2.9°S is obtained by the apparent polar wander path of India (Torsvik et al., 2012) for the reference point (29.8°N, 83.6°E) at ca. 75 Ma. The difference of the observed and expected paleolatitudes suggests that Greater India had a N-S extension of about 913 ± 374 km (8.3° ± 3.4°) at its central part at ca. 75 Ma for the reference point (29.8°N, 83.6°E), which is consistent with the N-S extension of 858 ± 374 km (7.8° ± 3.4°) at its eastern part calculated for the reference point (28.9°N, 89.2°E) (Yuan et al., 2021) (Fig. 10). Thus, our results indicate that Greater India had a similar magnitude of N-S extension during the middle Campanian at its central and eastern parts (Fig. 10). Our results further imply that Greater India had a similar extension of 860–910 km during the Early Cretaceous, which is well consistent (within errors) with previously obtained paleomagnetic results (Klootwijk and Bingham, 1980; Huang et al., 2015; Yang et al., 2015; Ma et al., 2016; Bian et al., 2019, 2022).

5.2. Geologic and geophysical evidence for the narrow Greater India

Our Greater India reconstruction is consistent with reconstructions based on balanced cross section constructions through the Himalayan fold-thrust belt (DeCelles et al., 2002; Long et al., 2011; Webb, 2013), seismologic studies across the Himalaya (Zhao et al., 2010; Gao et al., 2016; Guo et al., 2017; Zheng et al., 2020; Kufner et al., 2021), numerical modeling results (Zhou and Su, 2019; Liu et al., 2021; Li et al., 2022), and east Gondwana reconstructions (Ali and Aitchison, 2005). We discuss here the main observations and arguments of these earlier analyses in the frame of our refined Campanian configuration.

5.2.1. Balanced cross section constructions

A minimum shortening estimate of ~700–1100 km occurred in the Himalayan fold-thrust belt (e.g., DeCelles et al., 2002; Long et al., 2011; Webb, 2013) and this range of values is compatible with our paleomagnetically reconstructed magnitude (860–910 km) of Greater India size. DeCelles et al. (2002) made a regional compilation of shortening estimates along the Himalayan fold-thrust belt from Pakistan to Sikkim and reported that the total minimum shortening is up to ~670 km; and total shortening is greatest in northwestern India and Nepal. Later, Long

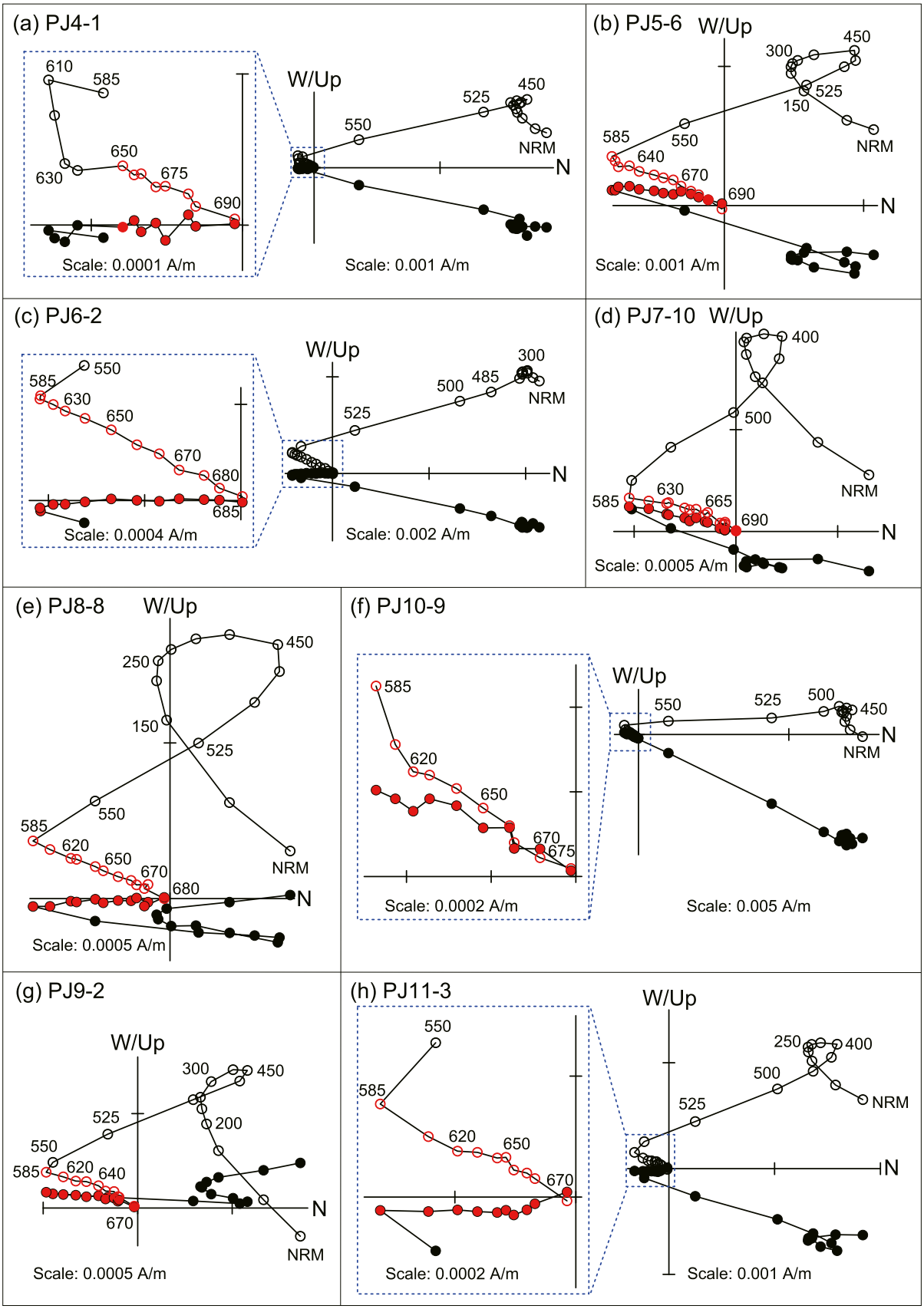

Fig. 6. Orthogonal demagnetization diagrams, all in thermal demagnetization, in geographic coordinates. The solid (open) circles represent projections on the horizontal (vertical) planes. The red data points were used for isolating the HTCs. The numbers refer to the temperatures in°C. NRM is the natural remanent magnetization.

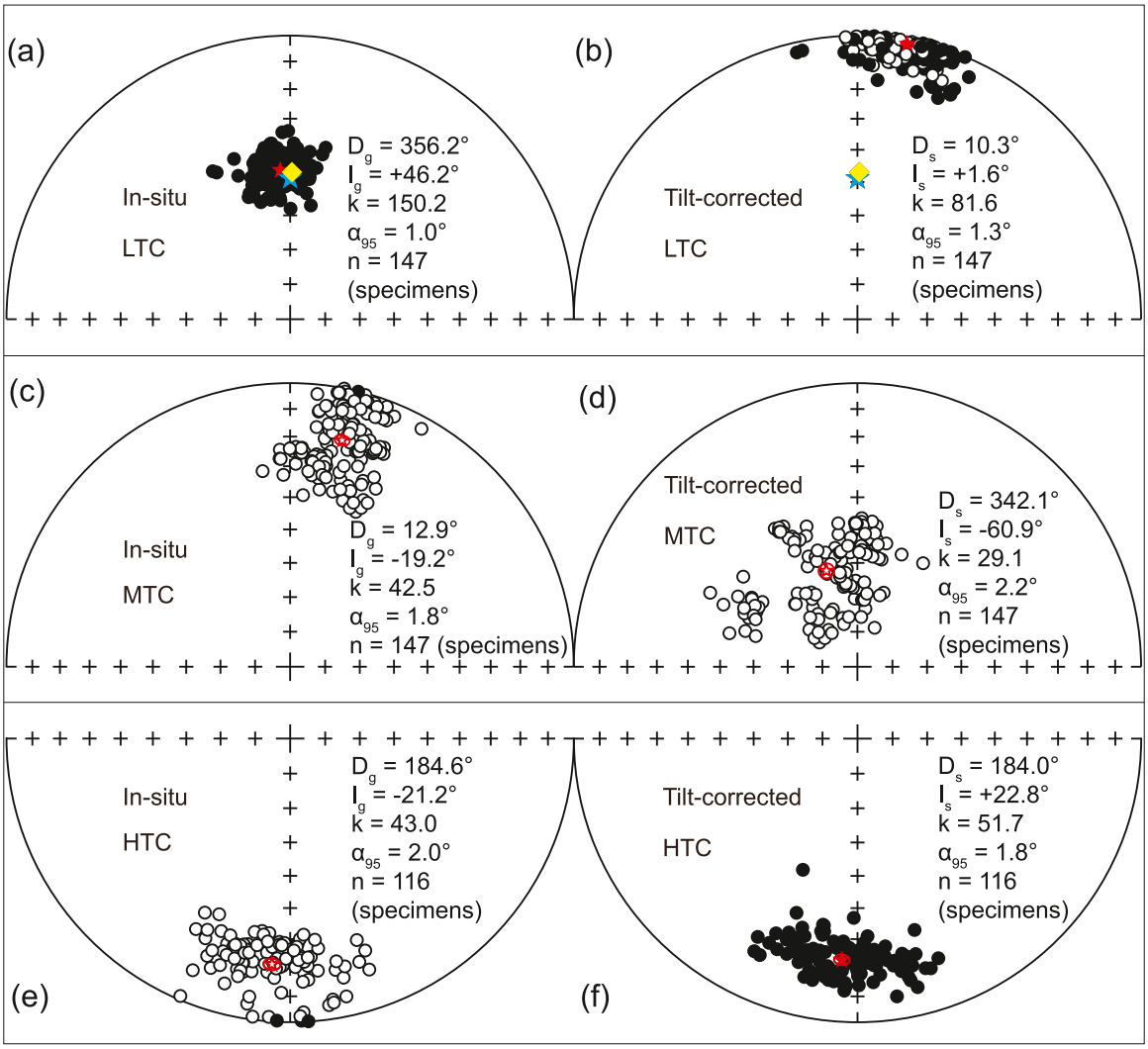

Fig. 7. Paleomagnetic results. (a–f) Equal-area projections of in-situ (left) and tilt-corrected (right) paleomagnetic directions of all specimens of the Pianji section. (a, b) LTC directions. (c, d) MTC directions. (e, f) HTC directions. Red circles around the red stars in the (a–f) denote the 95% confidence limit and mean directions. Solid and open symbols denote projections on the lower and upper hemisphere, respectively. The yellow diamonds and blue stars in the (a) and (b) denote the present geomagnetic field direction and the geocentric axial dipole direction of sampling section, respectively.

et al. (2011) presented four new balanced cross sections in Bhutan and surrounding regions, and updated a compilation of shortening estimates from west to east across the Himalayan fold-thrust belt after DeCelles et al. (2002). This updated compilation implied that the total minimum shortening is up to 919 km in Nepal; and the shortening magnitude corresponds to the classic "bow-and-arrow" model. Subsequently, Webb (2013) presented a line-length balanced section reconstruction across the Himalaya and calculated a minimum shortening estimate of 703–773 km across the western Himalaya. Because parts of the regional deformation could not be assessed, Webb (2013) suggested that estimates of ~900–1100 km more accurately reflect the minimum estimate shortening here.

5.2.2. Seismologic studies

A series of seismologic investigations of the presence of Indian continental crust beneath the Himalaya yield data that are consistent with our paleomagnetically determined narrow Greater India (Zhao et al., 2010; Gao et al., 2016; Guo et al., 2017; Zheng et al., 2020; Kufner et al., 2021).

In the western Himalayan syntaxis, only a part of Indian crust subducted to at least 160 km depth beneath the Hindu Kush, while the Indian mantle lithosphere subducted to a deeper position (Kufner et al., 2021). By contrast, to the east of the eastern Himalayan syntaxis, common conversion point images of receiver functions from a densely spaced seismic array revealed that the entire Indian crust with an average thickness of ~30 km had subducted to a depth of 100 km under central Myanmar (Zheng et al., 2020). In the central Himalaya, two profiles for the seismic discontinuities with the P and S receiver function techniques beneath central and western Tibet were presented (Zhao et al., 2010). Along the west line, the Indian lithospheric mantle gradually deepens from ~120 km depth in the south to ~200 km depth and remains horizontal up to 36°N; along the central line, the Indian lithospheric mantle deepens from ~100 km depth to ~200 km below the Bangong-Nujiang suture (Zhao et al., 2010).

Compared to the passive seismic methods, active source seismic probing is more likely to provide crustal structures with higher resolution (Gao et al., 2016). A seismic reflection profile across the western Yarlung Tsangpo suture zone at 81.5°E longitude clearly showed a continuous Moho reflection at ~70–75 km depth, which implies that no large-scale Indian crust had subducted into the mantle; on the contrary, only a small proportion of Indian continental lower crust had been underthrust beneath Asian continent farther north (Gao et al., 2016). Two new deep seismic reflection profiles across the central Yarlung Tsangpo suture zone at 88°E longitude also showed that Indian crust is

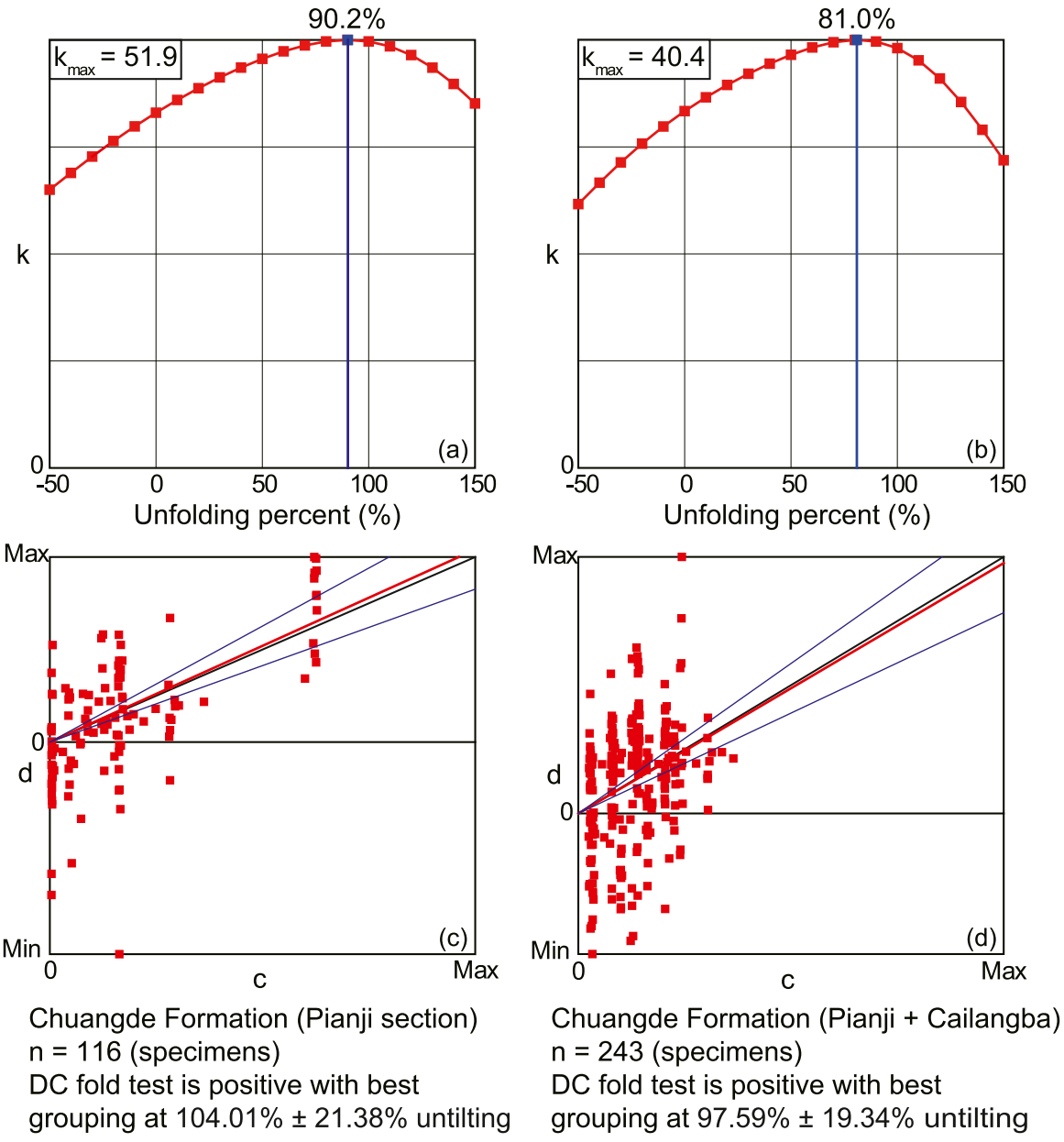

Fig. 8. Partial untilting test of Watson and Enkin (1993) and direction-correction (DC) fold test of Enkin (2003). (a, c) Positive fold tests (Watson and Enkin, 1993; Enkin, 2003) for the HTCs of the Chuangde Formation from the Pianji section in this study. (b, d) Positive fold tests (Watson and Enkin, 1993; Enkin, 2003) for the HTCs of the Chuangde Formation from the Pianji section in this study and the Cailangba section reported by Yuan et al. (2021). Fold tests are performed on the specimen level.

underthrust below southern Tibet. Combined with the seismic reflection profile of Gao et al. (2016), the new profiles reveal eastward steepening of the Indian crust underthrusting structure (Guo et al., 2017).

5.2.3. Numerical modeling

Our estimated narrow magnitude of Greater India reconstruction is also compatible with numerical modeling results (Zhou and Su, 2019; Liu et al., 2021; Li et al., 2022). First, crustal volume budget calculations show that no large magnitude of Indian continental crust subducted during the India-Asia collision (Zhou and Su, 2019). Second, numerical models were used to reproduce the relic Himalayan mass and they support a relatively small-sized Greater India rather than a larger extent of Greater India (Liu et al., 2021). Third, the convergence rate of the India-Asia collision was integrated into a large-scale thermomechanical numerical model (Li et al., 2022). The India-Asia collision at ≥55 Ma leads to significant continental shortening of ~2,900–4,000 km, which is hard to reconcile with the present-day Tibetan Plateau; thus, an oceanic basin and/or an intra-oceanic arc are required (Jagoutz et al., 2015; Li et al., 2022).

5.2.4. East Gondwana reconstructions

The extent of Greater India determined in this study is also consistent with the paleogeographic reconstructions of the western margin of the Australian continent based on the sub-continent's pre-breakup position within Gondwana and on the present-day bathymetry of the Indian Ocean to the west of Australia (Ali and Aitchison, 2005). Powell et al. (1988) made a major contribution to the reconstruction of eastern Gondwana and the India-Australia-Antarctica break-up history. Based on Powell et al.'s (1988) reconstruction, Ali and Aitchison (2005) suggested that Greater India only extended to the Wallaby-Zenith fracture zone. To the north of the Wallaby-Zenith fracture zone, the presence of continental crust of the Wallaby-Zenith plateaus effectively constrained

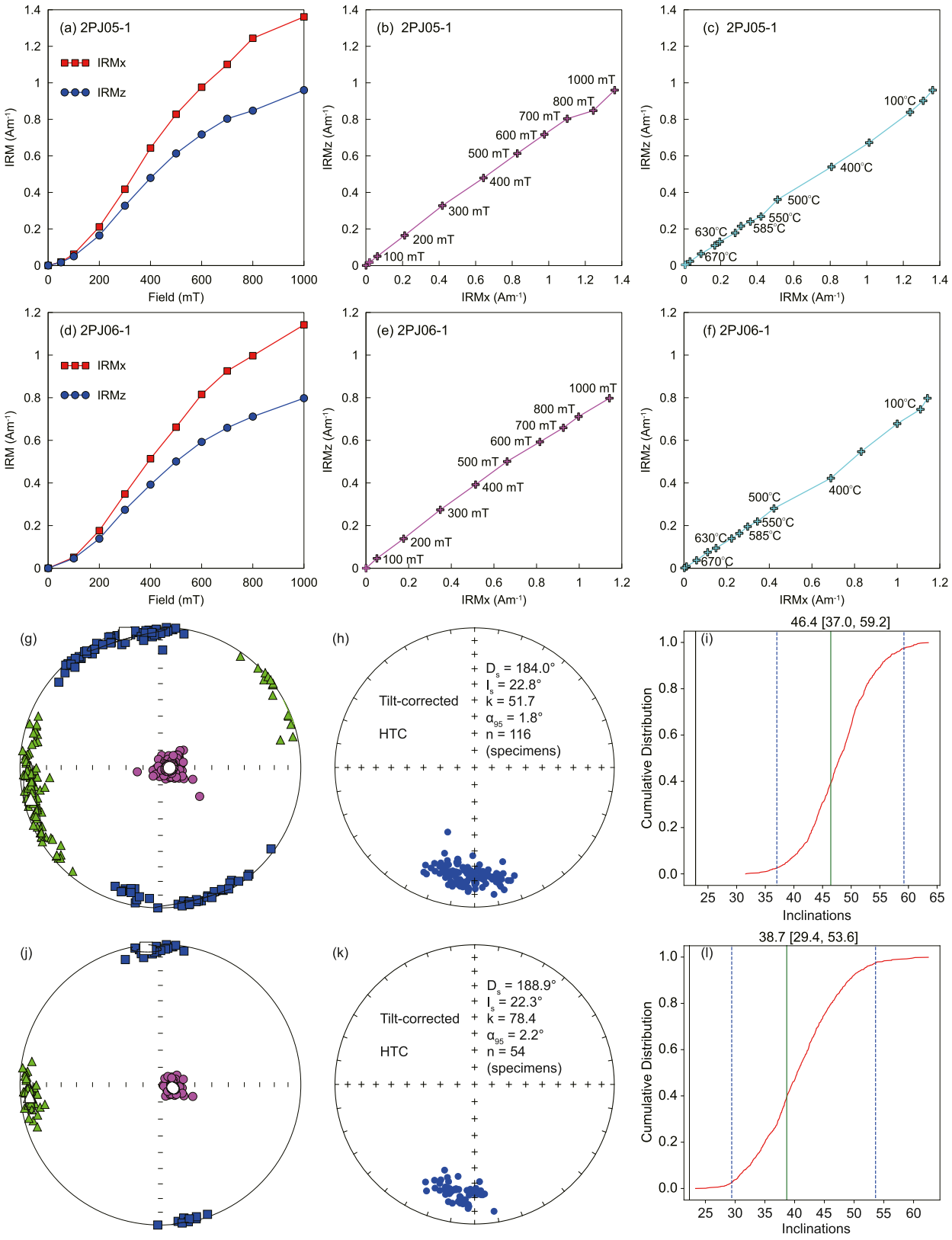

Fig. 9. The IRM anisotropy-based and the E/I inclination shallowing corrections. (a, d) The IRMx (parallel to bedding) and IRMz (perpendicular to bedding) acquisitions produced by applying a magnetic field at an angle of 45° to the bedding as a function of increasing field. (b, e) The slope (IRMz/IRMx) of the least-squares-fit for the data points between 0 mT and 1000 mT. (c, f) The slope of the thermal demagnetization of IRMz and IRMx, respectively. (g, j) The equal-area projections of the maximum (blue squares), intermediate (green triangles) and minimum (purple circles) susceptibility axes in stratigraphic coordinates. (h, k) The equal-area projections of samples directions. (i, l) The cumulative distribution of corrected inclination.

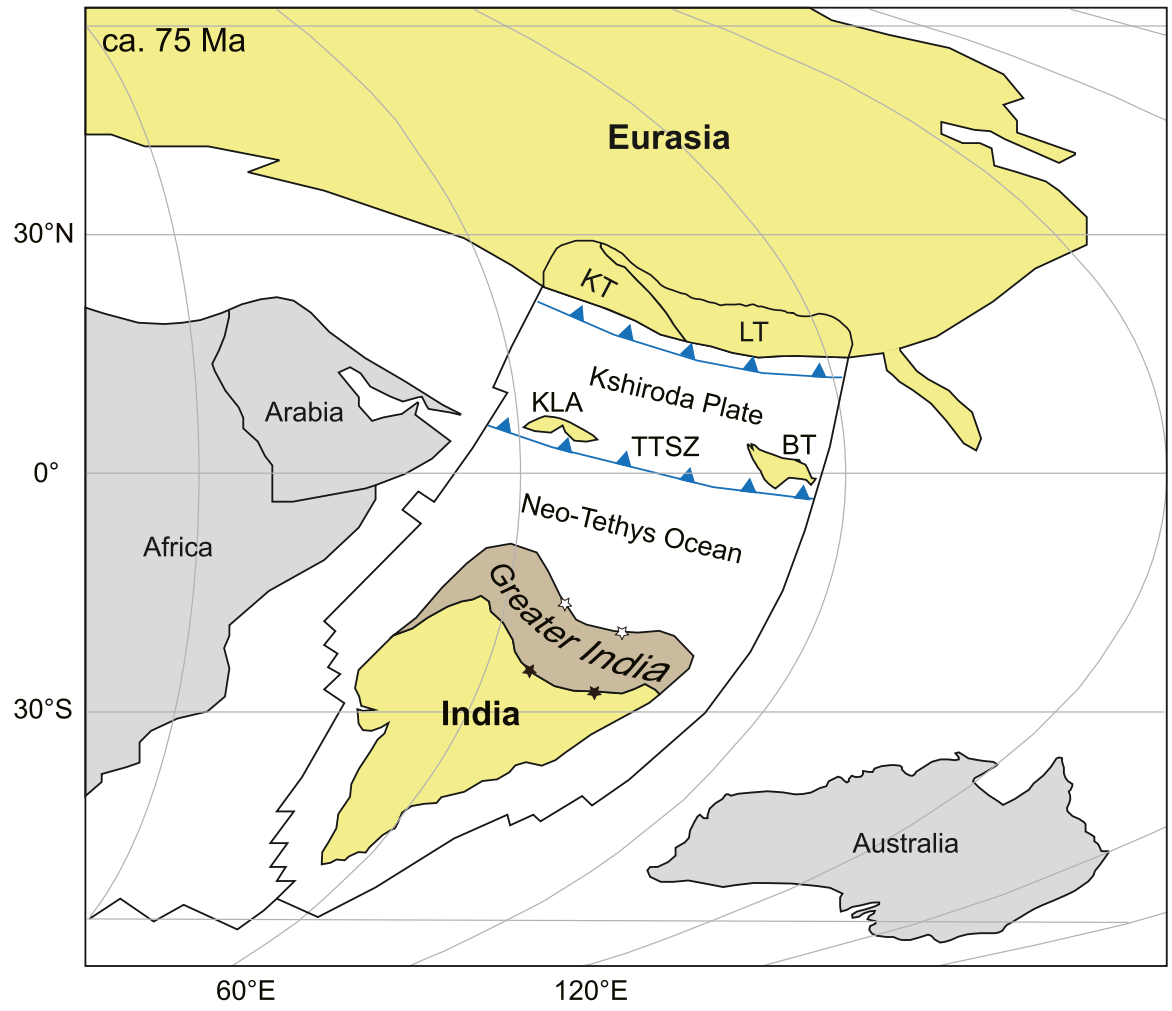

Fig. 10. Paleogeographic reconstruction of Greater India at ca. 75 Ma. Paleogeographic reconstruction based on the new (this study) and published (Yuan et al., 2021) paleomagnetic results of the Chuangde Formation CORBs in the Pianji section (this study) and the Cailangba section (Yuan et al., 2021) in southern Tibet, combined with the results of the Paleocene Khardung volcanic rocks on the Kohistan-Ladakh arc in Ladakh (Martin et al., 2020), of the Cretaceous red beds on the Kohistan-Ladakh arc in Kohistan (Zaman and Torii, 1999), of the upper Cretaceous strata in the Wuntho Range, Burma (Westerweel et al., 2019), of the Cretaceous–Paleocene strata on the Lhasa terrane (Tong et al., 2019), and of the upper Cretaceous rocks on the Karakoram terrane (Martin et al., 2021). The solid stars indicate the reference points (29.8°N, 83.6°E) and (28.9°N, 89.2°E) when calculating the extent of Greater India at its central and eastern parts, respectively. The open stars indicate the observed paleolatitudes from the Chuangde Formation CORBs in Zhongba and Gyangze, respectively. The Kshiroda Plate proposed by Jagoutz et al. (2015) is the oceanic plate between the northern and southern subduction systems. LT, Lhasa terrane. KT, Karakoram terrane. KLA, Kohistan-Ladakh arc. TTSZ, Trans-Tethyan subduction zone. BT, Burma terrane.

the extent of eastern Greater India to less than 950 km (Ali and Aitchison, 2005).

5.3. *Geologic arguments against a narrow Greater India and the North India Sea hypothesis*

Geologic arguments against a narrow Greater India and the North India Basin/Sea have previously been extensively discussed in several research and overview papers (e.g., Yin and Harrison, 2000; Webb, 2013; Ding et al., 2022). The most important drawbacks are that, up to now, no evidence exists for a second, younger, suture (Yin and Harrison, 2000; Webb, 2013) to support the presence of an ocean basin, such as the Greater India Basin of van Hinsbergen et al. (2012, 2019) or the North India Sea of Yuan et al. (2021, 2022) and no geologic evidence exists for the presence of an intra-oceanic arc in the central Himalaya (Yin, 2006). So far, there are no Cretaceous oceanic crustal (e.g. ophiolites) deposits found along the Main Central Thrust (MCT, Fig. 1).

Recently, van Hinsbergen (2022) explained why the absence of these deposits at the MCT is not an argument against the once-presence of a suture zone there. The hanging-wall of the MCT was, until activation of the MCT, resting on a section of rock that has been transferred farther below the orogen when the Greater Himalaya was extruded, and placed onto the Lesser Himalaya. Any accretionary prism formed structurally below the Greater Himalayan sequence would therefore have been transported deeper below the orogen – essentially by out-of-sequence thrusting (which is invoked in any extrusion model). Several other studies confirm that the use of ophiolites as marker of plate suture zones encounters challenges, especially for orogenic belts that have undergone long-term subduction-accretion processes, such as the Central Asian orogenic belt (Xiao et al., 2014), the Cordillera orogenic belt, and the Southeast Asian orogenic belt (Hall, 2017), as well as orogenic belts that have undergone strong collision processes, such as the Himalayan orogenic belt (Xiao et al., 2017). We consider it likely that remnants of the inferred intra-oceanic arc are still unidentified due to its fragmentary nature in the accretionary mélange (Martin et al., 2020). On these topics, we agree with the statement by Ding et al. (2022) that "*all current India-Asia suturing models have weaknesses. The community must continue to seek more certainty, such as if a ≤60 Ma oceanic basin existed between India and Asia, it is possible that scraps of it will be found, either in situ, as erosional remnants in the sedimentary record, or as xenoliths*". Thus, more

evidence from geologic investigations is required to further strengthen the proposed North India Sea hypothesis. Besides, more high-quality paleomagnetic data are also required to accurately delineate the India-Asia collision process.

5.4. Implications for the Tethyan paleogeography, the India-Asia collision and the behaviors of Indian continental crust

5.4.1. Tethyan paleogeography and India-Asia convergence

Our data provide stringent constraints on the latitudinal position of the central Tethyan Himalaya, the extent of Greater India and the size of the Neo-Tethys Ocean during the middle Campanian. The central Tethyan Himalaya was situated at a paleolatitude of ~17°S at ca. 75 Ma, suggesting that central Greater India had a N-S extension of ~910 km. Our data also imply that Greater India (with the rest of India) was far away from the Lhasa terrane during the middle Campanian; and that these elements were separated by the >3000 km wide Neo-Tethys Ocean (Fig. 10).

The North India Sea hypothesis and associated triple-stage collision scenario were put forward based on rapid changes in the paleo-latitudinal locations of the Tethyan Himalaya (Yuan et al., 2021, 2022). Clearly, the North India Sea hypothesis hinges on the reliability of the estimates for the N-S extent of Greater India at different longitudes. The new paleomagnetic data fill in the gap in the paleomagnetic dataset from the central part of the Tethyan Himalaya, and further provide critical constraints on the proposed North India Sea scenario (Yuan et al., 2021). Meanwhile, combining the recently published paleomagnetic data from the Kohistan-Ladakh arc in Ladakh (Martin et al., 2020) with the two prominent parallel slab remnants with high velocities beneath the Myanmar terrane (Yang et al., 2022), multiple subduction systems should be considered in the India-Asia collision system, as originally suggested by Jagoutz et al. (2015). Correspondingly, our proposed triple-stage collision scenario could be favorably considered in future studies of the Himalayan orogeny.

5.4.2. Implications for the behaviors of Indian continental crust

In the post-collisional period, buoyant upper crust of continental Greater India has been decoupled to be incorporated in the Himalayan fold-thrust belt. The Himalaya contains accreted continental upper crust of ~700–1100 km when restored to its undeformed state (DeCelles et al., 2002; Long et al., 2011; Webb, 2013), which is of equal dimension of our estimated Greater India. Only a small proportion of the rest of Indian crust is underthrust beneath the Lhasa terrane farther north; however, a large fraction of the rest of Indian crust was transferred into the overlying tectonic wedge of Webb et al. (2007) through crustal-scale duplexing and exhumation (Gao et al., 2016). The tectonic-wedge model suitably explains the change in structural correlation between the Himalayan units (Lesser Himalaya, Greater Himalaya, and Tethyan Himalaya) and the major Himalayan faults (the South Tibet Detachment System and the Main Central Thrust): the Main Central Thrust places the Greater Himalaya over the Lesser Himalaya in the central Himalaya, but it juxtaposes the Tethyan Himalaya over the Lesser Himalaya in the western Himalaya (Yin, 2006; Webb et al., 2007). This variation could be attributed to an eastward increase in the magnitude of duplexing and exhumation (Webb et al., 2007). The Indian crust has been partially subducted in the western Himalaya (Kufner et al., 2021), which consumed partial Indian crust. Consequently, a lesser amount of Indian crust is transferred into the overlying tectonic wedge in the western Himalaya, which could be the main cause of westward decrease in the magnitude of duplexing and exhumation. Subsequently, the spatially varying erosion resulted in the present-day topography of the Himalaya and Tibetan Plateau.

6. Conclusions

We have presented high-resolution thermal demagnetization data from the Chuangde Formation CORBs in the central Tethyan Himalaya located at 83.6°E longitude. Combined positive fold tests, rock magnetic analyses and petrographic observations suggest that the HTCs are of a relatively primary origin, and that the remanence is carried by detrital hematite of coarse-grained nature. After inclination shallowing correction, we provide a Campanian paleopole of 43.3°N/258.3°E, $A_{95} = 1.8°$, with a paleolatitude of 16.7° ± 1.8°S. Combining our results with paleomagnetic data from the Chuangde Formation CORBs in eastern Tethyan Himalaya at 89.2°E longitude, we conclude that Greater India during the Campanian had comparable N-S extents of ~910 km and ~860 km at its central and eastern parts, respectively. This estimate of Greater India extent is well consistent with multiple lines of geologic and geophysical evidence, and provides crucial insights into the geologic evolution of the India-Asia collision system.

CRediT authorship contribution statement

Jie Yuan: Writing – review & editing, Writing – original draft, Visualization, Methodology, Investigation, Funding acquisition, Formal analysis, Conceptualization. **Chenglong Deng:** Writing – review & editing, Supervision, Project administration, Investigation, Funding acquisition, Formal analysis, Conceptualization. **Zhenyu Yang:** Writing – review & editing, Methodology, Investigation, Funding acquisition, Formal analysis. **Wout Krijgsman:** Writing – review & editing, Methodology, Investigation, Formal analysis. **:** . **Huafeng Qin:** Methodology. **Liang Yi:** Investigation. **Pan Zhao:** Writing – review & editing. **Bo Wan:** Writing – review & editing. **Liang Zhao:** Writing – review & editing. **Huaiyu He:** Investigation. **Zhengtang Guo:** Supervision, Funding acquisition. **Rixiang Zhu:** Supervision.

CRediT authorship contribution statement

Jie Yuan: Writing – review & editing, Writing – original draft, Visualization, Methodology, Investigation, Funding acquisition, Formal analysis, Conceptualization. **Chenglong Deng:** Writing – review & editing, Supervision, Project administration, Investigation, Funding acquisition, Formal analysis, Conceptualization. **Zhenyu Yang:** Writing – review & editing, Methodology, Investigation, Funding acquisition, Formal analysis. **Wout Krijgsman:** Writing – review & editing, Methodology, Investigation, Formal analysis. **:** . **Huafeng Qin:** Methodology. **Liang Yi:** Investigation. **Pan Zhao:** Writing – review & editing. **Bo Wan:** Writing – review & editing. **Liang Zhao:** Writing – review & editing. **Huaiyu He:** Investigation. **Zhengtang Guo:** Supervision, Funding acquisition. **Rixiang Zhu:** Supervision.

Declaration of Competing Interest

The authors declare that they have no known competing financial interests or personal relationships that could have appeared to influence the work reported in this paper.

Data availability

Data will be made available on request.

Acknowledgements

J.Y. thanks Dr. Xi Chen for kindly providing stratigraphic information of the Chuangde Formation CORBs exposed in Zhongba. We sincerely acknowledge great assistance from Editor Hans Thybo, who handled an early version of this manuscript. We are very grateful to Dr. John W. Geissman and Editor Jean-Philippe Avouac for their insightful comments and suggestions to improve the quality of this manuscript. Thanks go also to Dr. An Yin for his critical but helpful review. Financial support was provided by the National Natural Science Foundation of

China (42104067, 41888101 and 91855216) and the China Postdoctoral Science Foundation (2021M693152 and 2023T160638).

Supplementary materials

Supplementary material associated with this article can be found, in the online version, at doi:10.1016/j.epsl.2023.118422.

References

Aitchison, J.C., Ali, J.R., Davis, A.M., 2007. When and where did India and Asia collide? J. Geophys. Res. 112, B05423. https://doi.org/10.1029/2006JB004706.

Ali, J.R., Aitchison, J.C., 2005. Greater India. Earth-Sci. Rev. 72, 169–188. https://doi.org/10.1016/j.earscirev.2005.07.005.

Argand, E., 1924. La tectonique de l' Asie. In: Proc. 13th Int. Geol. Cong., 7, pp. 181–372.

Bian, W., Yang, T., Ma, Y., Jin, J., Gao, F., Wang, S., Peng, W., Zhang, S., Wu, H., Li, H., Cao, L., 2019. Paleomagnetic and geochronological results from the Zhela and Weimei Formations lava flows of the eastern Tethyan Himalaya: new insights into the breakup of eastern Gondwana. J. Geophys. Res.: Solid Earth 124, 44–64. https://doi.org/10.1029/2018JB016403.

Bian, W., Yang, T., Wang, S., Peng, W., Zhang, S., Wu, H., Li, H., Zhao, P., 2022. Cretaceous paleomagnetic and detrital zircon U-Pb geochronological results from the Tethyan Himalaya: constraints on the Neo-Tethys evolution. Glob. Planet. Change 216, 103903. https://doi.org/10.1016/j.gloplacha.2022.103903.

Chen, X., Wang, C., Kuhnt, W., Holbourn, A., Huang, Y., Ma, C., 2011. Lithofacies, microfacies and depositional environments of Upper Cretaceous Oceanic red beds (Chuangde Formation) in southern. Tibet. Sed. Geol. 235, 100–110. https://doi.org/10.1016/j.sedgeo.2010.06.008.

Copley, A., Avouac, J.P., Royer, J.Y., 2010. India-Asia collision and the Cenozoic slowdown of the Indian plate: Implications for the forces driving plate motions. J. Geophys. Res. 115, B03410. https://doi.org/10.1029/2009JB006634.

Dannemann, S., Appel, E., Rösler, W., Neumann, U., Liebke, U., Nag, D., 2022. Palaeomagnetic indication for India-Asia collision at 12°N and maximum 810 km Greater India extent in the western suture zone. Geophys. J. Int. 229, 1193–1211. https://doi.org/10.1093/gji/ggab528.

DeCelles, P.G., Robinson, D.M., Zandt, G., 2002. Implications of shortening in the Himalayan fold-thrust belt for uplift of the Tibetan plateau. Tectonics 21, 1062. https://doi.org/10.1029/2001TC001322.

Ding, L., Kapp, P., Cai, F., Garzione, C.N., Xiong, Z., Wang, H., Wang, C., 2022. Timing and mechanisms of Tibetan Plateau uplift. Nat. Rev. Earth Env. 3, 652–667. https://doi.org/10.1038/s43017-022-00318-4.

Ding, L., Maksatbek, S., Cai, F., Wang, H., Song, P., Ji, W., Xu, Q., Zhang, L., Muhammad, Q., Upendra, B., 2017. Processes of initial collision and suturing between India and Asia. Sci. China Earth Sci. 60, 635–651. https://doi.org/10.1007/s11430-016-5244-x.

Du, X., Chen, X., Wang, C., Wei, Y., Li, Y., Jansa, L., 2015. Geochemistry and detrital zircon U-Pb dating of Lower Cretaceous volcaniclastics in the Babazhadong section, Northern Tethyan Himalaya: Implications for the breakup of Eastern Gondwana. Cretaceous Res 52, 127–137. https://doi.org/10.1016/j.cretres.2014.08.002.

Enkin, R.J., 2003. The direction-correction tilt test: an all-purpose tilt/fold test for paleomagnetic studies. Earth Planet. Sci. Lett. 212, 151–166. https://doi.org/10.1016/S0012-821X(03)00238-3.

Fisher, R.A., 1953. Dispersion on a sphere. Proc. R. Soc. Lond. 217, 295–305. https://doi.org/10.1098/rspa.1953.0064.

Gao, R., Lu, Z., Klemperer, S.L., Wang, H., Dong, S., Li, W., Li, H., 2016. Crustal-scale duplexing beneath the Yarlung Zangbo suture in the western Himalaya. Nat. Geosci. 9, 555–560. https://doi.org/10.1038/NGEO2730.

Guo, X., Li, W., Gao, R., Xu, X., Li, H., Huang, X., Ye, Z., Lu, Z., Klemperer, S.L., 2017. Nonuniform subduction of the Indian crust beneath the Himalayas. Sci. Rep. 7, 12497. https://doi.org/10.1038/s41598-017-12908-0.

Hall, R., 2017. Southeast Asia: new views of the geology of the Malay Archipelago. Annu. Rev. Earth Planet. Sci. 45, 331–358. https://doi.org/10.1146/annurev-earth-063016-020633.

Hodych, J.P., Buchan, K.L., 1994. Early Silurian palaeolatitude of the Springdale Group redbeds of central Newfoundland: a palaeomagnetic determination with a remanence anisotropy test for inclination error. Geophys. J. Int. 117, 640–652. https://doi.org/10.1111/j.1365-246X.1994.tb02459.x.

Hu, X., Wang, J., An, W., Garzanti, E., Li, J., 2017. Constraining the timing of the India-Asia continental collision by the sedimentary record. Sci. China Earth Sci. 60, 603–625. https://doi.org/10.1007/s11430-016-9003-6.

Huang, W., van Hinsbergen, D.J.J., Dekkers, M.J., Garzanti, E., Dupont-Nivet, G., Lippert, P.C., Li, X., Maffione, M., Langereis, C.G., Hu, X., Guo, Z., Kapp, P., 2015. Paleolatitudes of the Tibetan Himalaya from primary and secondary magneti-zations of Jurassic to Lower Cretaceous sedimentary rocks. Geochem. Geophys. Geosyst. 16, 77–100. https://doi.org/10.1002/2014GC005624.

Ingalls, M., Rowley, D.B., Currie, B., Colman, A.S., 2016. Large-scale subduction of continental crust implied by India-Asia mass-balance calculation. Nat. Geosci. 9, 848–853. https://doi.org/10.1038/NGEO2806.

Jagoutz, O., Royden, L., Holt, A.F., Becker, T.W., 2015. Anomalously fast convergence of India and Eurasia caused by double subduction. Nat. Geosci. 8, 475–478. https://doi.org/10.1038/ngeo2418.

Kapp, P., DeCelles, P.G., 2019. Mesozoic–Cenozoic geological evolution of the Himalayan-Tibetan orogen and working tectonic hypotheses. Am. J. Sci. 319, 159–254. https://doi.org/10.2475/03.2019.01.

Kirschvink, J.L., 1980. The least-squares line and plane and the analysis of palaeomagnetic data. Geophys. J. Int. 62, 699–718. https://doi.org/10.1111/j.1365-246X.1980.tb02601.x.

Klootwijk, C.T., Bingham, D.K., 1980. The extent of greater India, III. Palaeomagnetic data from the Tibetan Sedimentary series, Thakkhola region. Nepal Himalaya. Earth Planet. Sci. Lett. 51, 381–405. https://doi.org/10.1016/0012-821X(80)90219-8.

Kruiver, P.P., Dekkers, M.J., Heslop, D., 2001. Quantification of magnetic coercivity components by the analysis of acquisition curves of isothermal remanent magnetisation. Earth Planet. Sci. Lett. 189, 269–276. https://doi.org/10.1016/S0012-821X(01)00367-3.

Kufner, S.K., Kakar, N., Bezada, M., Bloch, W., Metzger, S., Yuan, X., Mechie, J., Ratschbacher, L., Murodkulov, S., Deng, Z., Schurr, B., 2021. The Hindu Kush slab break-off as revealed by deep structure and crustal deformation. Nat. Commun. 12, 1685. https://doi.org/10.1038/s41467-021-21760-w.

Li, G., Jansa, L., Wan, X., Pan, M., Xiu, D., Xie, D., 2011. Discovery of radiolaria from Upper cretaceous oceanic red beds in Daba, Kangmar and its paleogeographic implication. Palaeogeogr. Palaeoclimatol. Palaeoecol. 312, 127–137. https://doi.org/10.1016/j.palaeo.2011.10.003.

Li, Q., Li, Z.H., Zhong, X., 2022. Overriding lithospheric strength affects continental collisional mode selection and subduction transference: Implications for the Greater India-Asia convergent system. Front. Earth Sci. 10, 919174 https://doi.org/10.3389/feart.2022.919174.

Li, X., Matsuoka, A., Li, Y., Wang, C., 2017. Phyletic evolution of the mid-Cretaceous radiolarian genus Turbocapsula from southern Tibet and its applications in zonation. Mar. Micropaleontol. 130, 29–42. https://doi.org/10.1016/j.marmicro.2016.11.002.

Liu, G., Einsele, G., 1994. Sedimentary history of the Tethyan basin in the Tibetan Himalayas. Geol. Rundsch. 83, 32–61. https://doi.org/10.1007/BF00211893.

Liu, L., Liu, L., Xu, Y.G., 2021. Intermittent post-Paleocene continental collision in South Asia. Geophys. Res. Lett. 48, e2021GL094531 https://doi.org/10.1029/2021GL094531.

Long, S.P., McQuarrie, N., Tobgay, T., Grujic, D., 2011. Geometry and crustal shortening of the Himalayan fold-thrust belt, eastern and central Bhutan. Geol. Soc. Am. Bull. 123, 1427–1447. https://doi.org/10.1130/B30203.1.

Lowrie, W., 1990. Identification of ferromagnetic minerals in a rock by coercivity and unblocking temperature properties. Geophys. Res. Lett. 17, 159–162. https://doi.org/10.1029/GL017i002p00159.

Ma, Y., Yang, T., Bian, W., Jin, J., Zhang, S., Wu, H., Li, H., 2016. Early Cretaceous paleomagnetic and geochronologic results from the Tethyan Himalaya: insights into the Neotethyan paleogeography and the India-Asia collision. Sci. Rep. 6, 21605. https://doi.org/10.1038/srep21605.

Martin, C.R., Jagoutz, O., Upadhyay, R., Mueller, P., Weiss, B.P., 2021. Paleomagnetism and geochronology of the Eurasian margin in the Shyok suture zone. In: Paper presented at GSA Connects Abstracts.

Martin, C.R., Jagoutz, O., Upadhyay, R., Royden, L.H., Eddy, M.P., Bailey, E., Nichols, C. I.O., Weiss, B.P., 2020. Paleocene latitude of the Kohistan-Ladakh arc indicates multistage India-Eurasia collision. Proc. Natl. Acad. Sci. U.S.A. 117, 29487–29494. https://doi.org/10.1073/pnas.2009039117.

McElhinny, M.W., 1964. Statistical significance of the fold test in paleomagnetism. Geophys. J. R. Astron. Soc. 8, 338–340. https://doi.org/10.1111/j.1365-246X.1964.tb06300.x.

McFadden, P.L., 1990. A new fold test for paleomagnetic studies. Geophys. J. Int. 103, 163–169. https://doi.org/10.1111/j.1365-246X.1990.tb01761.x.

Meng, J., Gilder, S.A., Wang, C., Coe, R.S., Tan, X., Zhao, X., He, K., 2019. Defining the limits of greater India. Geophys. Res. Lett. 46, 4182–4191. https://doi.org/10.1029/2019GL082119.

Molnar, P., Tapponnier, P., 1975. Cenozoic tectonics of Asia: effects of a continental collision. Science 189, 419–426. https://doi.org/10.1126/science.189.4201.419.

Néel, L., 1949. Théorie due trainage magnétique des ferromagnétiques en grains fins avec applications au terres cuites. Annales de Géophysique 5, 99–136.

Powell, C.M., Roots, S.R., Veevers, J.J., 1988. Pre-breakup continental extension in eastern Gondwanaland and the early opening of the eastern Indian Ocean. Tectonophysics 155, 261–283. https://doi.org/10.1016/0040-1951(88)90269-7.

Qin, H., Zhao, X., Liu, S., Paterson, G.A., Jiang, Z., Cai, S., Li, J., Liu, Q., Zhu, R., 2020. An ultra-low magnetic field thermal demagnetizer for high-precision paleomagnetism. Earth Planets Space 72, 170. https://doi.org/10.1186/s40623-020-01304-0.

Robertson, D.J., France, D.E., 1994. Discrimination of remanence-carrying minerals in mixtures, using isothermal remanent magnetisation acquisition curves. Phys. Earth Planet. Inter. 82, 223–234. https://doi.org/10.1016/0031-9201(94)90074-4.

Swanson-Hysell, N.L., Fairchild, L.M., Slotznick, S.P., 2019. Primary and secondary red bed magnetization constrained by fluvial intraclasts. J. Geophys. Res.: Solid Earth 124, 4276–4289. https://doi.org/10.1029/2018JB017067.

Tauxe, L., Kent, D.V., 2004. A simplified statistical model for the geomagnetic field and the detection of shallow bias in paleomagnetic inclinations: was the ancient magnetic field dipolar? In: Channell, J., Kent, D., Lowrie, W., Meert, J. (Eds.), Timescales of the Paleomagnetic Field. In: Geophysical Monograph Series 145, 101–115. https://doi.org/10.1029/145GM08.

Tauxe, L., Watson, G.S., 1994. The fold test: an eigen analysis approach. Earth Planet. Sci. Lett. 122, 331–341. https://doi.org/10.1016/0012-821X(94)90006-X.

Tong, Y., Yang, Z., Li, J., Pei, J., Li, J., 2019. New insights into the collision process of India and Eurasia: evidence from the syntectonic-sedimentation-induced

inclinational divergence of Cretaceous paleomagnetic data of the Lhasa Terrane. Earth-Sci. Rev. 190, 570–588. https://doi.org/10.1016/j.earscirev.2019.02.009.
Torsvik, T.H., van der Voo, R., Preeden, U., Niocaill, C.M., Steinberger, B., Doubrovine, P.V., van Hinsbergen, D.J.J., Domeier, M., Gaina, C., Tohver, E., Meert, J.G., McCausland, P.J.A., Cocks, L.R.M., 2012. Phanerozoic polar wander, palaeogeography and dynamics. Earth-Sci. Rev. 114, 325–368. https://doi.org/10.1016/j.earscirev.2012.06.007.
van Hinsbergen, 2022. Indian Plate paleogeography, subduction, and horizontal underthrusting below Tibet: paradoxes, controvercies, and opportunities. Natl. Sci. Rev. 9, nwac074. https://doi.org/10.1093/nsr/nwac074.
van Hinsbergen, D.J.J., Lippert, P.C., Dupont-Nivet, G., McQuarrieh, N., Doubrovine, P. V., Spakman, W., Torsvik, T.H., 2012. Greater India Basin hypothesis and a two-stage Cenozoic collision between India and Asia. Proc. Natl. Acad. Sci. USA 109, 7659–7664. https://doi.org/10.1073/pnas.1117262109.
van Hinsbergen, D.J.J., Lippert, P.C., Li, S., Huang, W., Advokaat, E.L., Spakman, W., 2019. Reconstructing Greater India: paleogeographic, kinematic, and geodynamic perspectives. Tectonophysics 760, 69–94. https://doi.org/10.1016/j.tecto.2018.04.006.
Watson, G.S., Enkin, R.J., 1993. The fold test in paleomagnetism as a parameter estimation problem. Geophys. Res. Lett. 20, 2135–2137. https://doi.org/10.1029/93GL01901.
Webb, A.A.G., 2013. Preliminary balanced palinspastic reconstruction of Cenozoic deformation across the Himachal Himalaya (northwestern India). Geosphere 9, 572–587. https://doi.org/10.1130/GES00787.1.
Webb, A.A.G., Yin, A., Harrison, T.M., Célérier, J., Burgess, W.P., 2007. The leading edge of the Greater Himalayan Crystalline complex revealed in the NW Indian Himalaya: implications for the evolution of the Himalayan orogen. Geology 35, 955–958. https://doi.org/10.1130/G23931A.1.
Westerweel, J., Roperch, P., Licht, A., Dupont-Nivet, G., Win, Z., Poblete, F., Ruffet, G., Swe, H.H., Thi, M.K., Aung, D.W., 2019. Burma Terrane part of the Trans-Tethyan arc during collision with India according to palaeomagnetic data. Nat. Geosci. 12, 863–868. https://doi.org/10.1038/s41561-019-0443-2.
Xiao, W., Ao, S., Yang, L., Han, C., Wan, B., Zhang, J., Zhang, Z., Li, R., Chen, Z., Song, S., 2017. Anatomy of composition and nature of plate convergence: insights for alternative thoughts for terminal India-Eurasia collision. Sci. China Earth Sci. 60, 1015–1039. https://doi.org/10.1007/s11430-016-9043-3.
Xiao, W., Han, C., Liu, W., Wan, B., Zhang, J., Ao, S., Zhang, Z., Song, D., Tian, Z., Luo, J., 2014. How many sutures in the southern Central Asian orogenic belt: insights from East Xinjiang-West Gansu (NW China)? Geosci. Front. 5, 525–536. https://doi.org/10.1016/j.gsf.2014.04.002.
Yang, S., Liang, X., Jiang, M., Chen, L, He, Y., Mon, C.T., Hou, G., Thant, M., Sein, K., Wan, B., 2022. Slab remnants beneath the Myanmar terrane evidencing double subduction of the Neo-Tethyan Ocean. Sci. Adv. 8, eabo1027. https://doi.org/10.1126/sciadv.abo1027.
Yang, T., Ma, Y., Bian, W., Jin, J., Zhang, S., Wu, H., Li, H., Yang, Z., Ding, J., 2015. Paleomagnetic results from the Early Cretaceous Lakang Formation lavas: constraints on the paleolatitude of the Tethyan Himalaya and the India–Asia collision. Earth Planet. Sci. Lett. 428, 120–133. https://doi.org/10.1016/j.epsl.2015.07.040.
Yin, A., 2006. Cenozoic tectonic evolution of the Himalayan orogen as constrained by along-strike variation of structural geometry, exhumation history, and foreland sedimentation. Earth-Sci. Rev. 76, 1–131. https://doi.org/10.1016/j.earscirev.2005.05.004.
Yin, A., Harrison, T.M., 2000. Geologic evolution of the Himalayan-Tibetan orogen. Annu. Rev. Earth Planet. Sci. 28, 211–280. https://doi.org/10.1146/annurev.earth.28.1.211.
Yuan, J., Deng, C., Yang, Z., Krijgsman, W., Thubtantsering, Qin, H., Shen, Z., Hou, Y., Zhang, S., Yu, Z., Zhao, P., Zhao, L., Wan, B, He, H., Guo, Z., 2022. Triple-stage India-Asia collision involving arc-continent collision and subsequent two-stage continent-continent collision. Glob. Planet. Change 212, 103821. https://doi.org/10.1016/j.gloplacha.2022.103821.
Yuan, J., Yang, Z., Deng, C., Krijgsman, W., Hu, X., Li, S., Shen, Z., Qin, H., An, W., He, H., Ding, L., Guo, Z., Zhu, R., 2021. Rapid drift of the Tethyan Himalaya terrane before two-stage India-Asia collision. Natl. Sci. Rev. 8, nwaa173. https://doi.org/10.1093/nsr/nwaa173.
Zaman, H., Torii, M., 1999. Palaeomagnetic study of Cretaceous red beds from the eastern Hindukush ranges, northern Pakistan: Palaeoreconstruction of the Kohistan-Karakoram composite unit before the India-Asia collision. Geophys. J. Int. 136, 719–738. https://doi.org/10.1046/j.1365-246x.1999.00757.x.
Zhao, J., Yuan, X., Liu, H., Kumar, P., Pei, S., Kind, R., Zhang, Z., Teng, J., Ding, L., Gao, X., Xu, Q., Wang, W., 2010. The boundary between the Indian and Asian tectonic plates below Tibet. Proc. Natl. Acad. Sci. USA 107, 11229–11233. https://doi.org/10.1073/pnas.1001921107.
Zheng, T., He, Y., Ding, L., Jiang, M., Ai, Y., Mon, C.T., Hou, G., Sein, K., Thant, M., 2020. Direct structural evidence of Indian continental subduction beneath Myanmar. Nat. Commun. 11, 1944. https://doi.org/10.1038/s41467-020-15746-3.
Zhou, J., Su, H., 2019. Site and timing of substantial India-Asia collision inferred from crustal volume budget. Tectonics 38, 2275–2290. https://doi.org/10.1029/2018TC005412.
Zhu, R., Zhao, P., Zhao, L., 2022. Tectonic evolution and geodynamics of the Neo-Tethys Ocean. Sci. China Earth Sci. 65, 1–24. https://doi.org/10.1007/s11430-021-9845-7.